Authors response to Anonymous Referee #1

Major comments:

1. **(Comment)** This paper describes an attempt by the authors to use gamma function fitted using cloud macro- and microphysical observations to analyze microphysical growing path and particle size distribution evolution within deep convective clouds. The data used in this study are from ACRIDICON-CHUVA field campaign over Amazon, primarily six flights focusing on cloud microphysics measurements over regions with different aerosol background profiles. The findings of cloud properties under different environments appear to be very interesting. However, the method in using gamma function to interpret cloud microphysical growing path contains serious issues.

1. **(Answer)** We would like to thank Anonymous Referee #1 for the invaluable comments. Please find in this document the detailed answers to your concerns.

2. **(Comment)** The description of the closure of gamma function was firstly given by Eq. (2) - (4), where the closure variables were the zeroth, second, and third moment. The three undetermined parameters of gamma function would be defined by these moments. However, the actual closure variables, as described in Eq. (6) – (8) are liquid water content, cloud droplet number concentration, and effective droplet diameter. The former two were equivalent to the third and zeroth moment, respectively, while the effective droplet diameter was mostly equivalent to the first moment. To the least, these two descriptions are redundant. In fact, in many places of the paper including the Concluding remarks, the authors were still referred to the second moment. Indeed, the procedure of fitting gamma function with observations was never clearly described.

2. **(Answer)** The third paragraph and Equations (2) – (4) explain the methodology adopted to obtain the Gamma parameters. It is a relatively simple process and the method of moments has been extensively

studied in the literature. From the Gamma parameters obtained with this methodology, we are able to calculate any DSD property of interest - note that the Gamma parameters fully define the respective Gamma DSD. In this study, we were interested in analyzing (among other things) the parameters given in Equations (6) – (9). Those are not closure parameters to obtain the Gamma DSD, instead are properties we obtain from them. Because we use moments of order 0, 2, and 3, N_d, LWC, and D_{eff} obtained from the Gamma parameters will exactly match the observations. The relative dispersion, on the other hand, have dependency on the first moments and will be slightly different. However, as explained in the text after Equations (6) – (9), this parameters is still well represented by the Gamma fit used here.

3. **(Comment)** The most serious flaw of the proposed method exists in the procedure to interpret microphysics in the phase space of size distribution function. For a given air parcel, the ternary group of closure variables (mostly moments in different order) and undetermined parameters are bonded by mass conservation applied to the prognostic procedure of the former group, this defines the unique solution of both groups through the evolution of the air parcel, and they change accordingly due to the variations of the closure variables induced by dynamical and microphysical processes. Note also that the closure variables must be conservative ones with well-defined sink and source besides advection and mixing terms. When fitting gamma function with multiple observations, however, one should realize that these observations are multiple snapshots likely represent different air mass origin either unmixed or mixed, therefore, they mostly reflect different ternary groups of the closure variables and hence their paths in the phase space are irrelevant microphysically speaking unless a strong isentropic assumption (at least for any given horizontal plane) is made. This is why even in analyzing Eulerian modeling results, modelers usually derive microphysical and size distribution evolution within a parcel framework (can be conveniently derived from Eulerian grid parameters though), e.g., the "Twomey model". Only within such a framework does the analysis of size distribution evolution become meaningful.

3. **(Answer)** We understand your concern because we are not strictly using a Lagrangian measurement setup (which is not possible using airplanes). As there is no way to follow specific air parcels with aircraft measurements, we had to steer our analysis to get as close as possible to the cloud evolution. Firstly, the

flight patterns were specifically chosen as to measure growing convective clouds at their tops. Therefore, in each vertical step of the aircraft, we probed clouds that were "older" than the clouds probed on the last step (vertical steps were in ascending order). Additionally, the Gamma phase-space trajectories are only calculated for $w > 0$ m s^{-1}, making sure we only capture the growing part of the convective elements. The flight strategy is now clarified in Section 2.1, where we added the following sentence (second paragraph): "The latter step was deployed as follows. After the cloud base penetration, the aircraft performed several penetrations in vertical steps of several hundred meters. In each step, the aircraft penetrated the cloud tops available, thus avoiding precipitation from above. In this way, different clouds can be penetrated in the same altitude level and the vertical steps followed the growing cumuli field overall". This procedure was performed to allow interpreting the data (only w>0) as quasi-Lagrangian trajectories of the cloud parcels. We also performed simple calculations with the help of a Lagrangian parcel model. For details of the runs, please refer to our answers to Anonymous Referee #2 (item 2). Overall, the model calculations show that the condensation and collision-coalescence pseudo-forces act in similar directions to what we show in Figure 3. Therefore, we not only provide further justifications for Figure 3, but also show that the trajectories in Figures 5-8 can also be explained by the physical processes in the Lagrangian model. Of course, the Lagrangian model we chose is relatively simple given that it does not consider advection or turbulent mixing. On the other hand, it is capable of isolating the effects of condensation and collision-coalescence growth on the DSDs (bin microphysics) and, therefore, on the trajectories in the Gamma phase-space. The fact that we observed similarities between the Lagrangian trajectories and the observed ones is a strong argument in favor of our approach.

4. **(Comment)** By the way, many comments made by the authors are not accurate. For example, in the Abstract, the opening statement seems attempting to link our lack of understanding of the "tropical clouds" solely to the model representation issue of certain physical processes. The statement of "there is almost no study dedicated to understanding the phase space of this function…" is not accurate too. The properties of Gamma function along with many other probability distributions have been well studied and documented in statistics and applied mathematics literature. In the cloud physics and modeling field, the

evolution of conservative moments (mostly in the format of LWC, number concentration, and spectral disperse) have never been a rare topic in various mostly modeling studies.
The observations are invaluable for further our understanding of cloud physics and for evaluating models. Applying derivatives of these data, however, warrens special cautiousness.

4. **(Answer)** Yes, we agree that the phrasing regarding tropical clouds and their representation in models was not appropriate. The intended meaning is that, because of our lack of knowledge of tropical clouds, we still can't reproduce them adequately in models. We changed the first sentence in the Abstract to be: "The behavior of tropical clouds remains a major open scientific question, resulting in poor representation by models".
We also updated the Gamma function reference in the Abstract to: "However, even though the statistical characteristics of the Gamma parameters have been widely studied, there is almost no study dedicated to understanding the phase space of this function and the associated physics. This phase space can be defined by the three parameters that define the DSD intercept, shape, and curvature…".

Authors response to Anonymous Referee #2

Major comments:

1. **(Comment)** This manuscript introduces a technique for describing cloud processes using the drop size distribution gamma fit coefficients, and the trajectory of these coefficients in three-dimensional space. Comparisons within this phase space are made among clouds with different environmental conditions and linked to various cloud processes. While the manuscript is well written, I think some aspects of the paper need further work.

1. **(Answer)** We thank Anonymous Referee #2 for the invaluable comments. Please find in this document the detailed responses to your concerns.

2. **(Comment)** First, the physical insights that are provided are not closely linked to the coefficients themselves, and instead are reworked into pseudo-forces related to condensation and collision processes. However, the method used to decompose the trajectories into these pseudo forces is not clearly described, and as a result I find it difficult to accept many of the explanations behind the patterns in the data.

2. **(Answer)** Indeed, the pseudo-forces presented are somewhat loosely defined, which is one of the main reasons why we use "Illustration of microphysical processes…" in the title. The use of the Gamma phase space as an entity is new to the microphysical studies and we do not aim to cover all its aspects in this first introduction. We are already working in a new study focusing only on cloud modeling to extract the pseudo-forces definition and to show how this approach can be useful for microphysical modeling. In this study, our main interest is to show that we can study patterns in this space and that it can be useful to the tools already implemented in models (or remote sensing applications) and to develop new ones.

That said, we followed your suggestion and dedicated efforts to better define and quantify the pseudo-forces properties. We identified that the ideal tool to address this issue would be a relatively simple model that solves the condensation and collision-coalescence growth using the bin approach instead of the bulk. A model that fits those requirements is described in Feingold et al. (1999) – item "c" in section 3, where we run only two parcels and not a bigger ensemble. This is a parcel model that treats the DSDs in 35 mass-doubling bins from 3.5 μm up to ~9 mm in diameter. The processes solved by the model are: 1) CCN activation, considered to be composed of ammonium sulfate; 2) growth by condensation; 3) growth by collision-coalescence and 4) effects of giant CCN on the DSD evolution (we turn this process off for the purposes of this review). Other processes such as aqueous chemistry, complex aerosol composition, trace gases and radiation (and the effects of those processes on the DSDs) are not treated. Additionally, by being a parcel model, it does not consider turbulent mixing and sedimentation from above.

The characteristics of the model make it suitable to simulate the effects of condensation and collision-coalescence growth in the DSDs, which we can use to show the related patterns in the Gamma phase-space. We tried to produce results based on the conditions measured during flight AC09 (now RA1), where we used the following parameters as input: 1) mean aerosol diameter D_g = 1.55 μm, with standard deviation of 2.2 for the lognormal function of the aerosols; 2) pressure at cloud base of 890 hPa; and 3)

temperature at cloud base of 20.85 °C. The vertical speed was fixed at 0.5 m s^{-1} as we wanted to minimize the effect of new droplet formation in the DSD shape. Under those conditions, we ran the model twice: one run with only condensational growth (CG run) and one with both condensation and collision-coalescence growth (C2G run). Both runs produced the exact same DSDs in the lower parts of the cloud where the condensation dominates, but differed significantly when the collision-coalescence became active (around 1200 m, where cloud base is at 0 m). When the collision-coalescence process activates, $D_{eff} \approx 25$ µm and the condensational growth is much less effective. Therefore, it was possible to isolate both processes. Because there is no turbulent mixing or dilution with dry air, the droplet growth with altitude is much more pronounced in the model compared to our measurements during AC09. For this reason, we do not limit the Gamma fit to D < 50 µm as in the paper. Otherwise, it would be difficult to capture the effects of the collision-coalescence process – droplets grow relatively quickly beyond the 50 µm mark.

We fitted Gamma DSDs (using the same moments of order zero, two, and three as in the paper) to the model outputs every 20 seconds. Therefore, each point in the Gamma phase space represents the instantaneous DSD measured every 20 seconds. The results are shown in the following three figures.

Figure R1 shows the Gamma phase space for both runs, where "*" markers are related to CG run and squares to C2G. The arrows represent the displacement vector every 20 seconds, which is related to the respective pseudo-force (colors represent altitude above cloud base in m). Note that in the first 500 m the Gamma points are the same for both runs. This layer is defined by condensational growth alone and we observe a "zig-zag" pattern in the Gamma phase-space. When the trajectory is upwards in the "zig-zag", they are similar to what we observed in the paper – that is, growing µ and Λ (and shrinking N_0) along with the condensational growth. On the other hand, the model results also show a downward (in the Gamma space) trend during condensational growth. We noted that when the trajectory is downwards, the Gamma fit does not represent the DSD width correctly. At those points, the fixed bins between 10 µm and 15 µm present fast-growing concentrations (when the droplets grow sufficiently to transition from the lower bins) that disproportionately affects the Gamma DSD width. In the downward pattern, the Gamma DSD relative dispersion can be up to 150% higher than the binned DSD. When the process sta-

bilizes, the trajectory returns to the upward trend and the Gamma and binned DSD widths get progressively closer (~20% to ~50% difference). Based in those results we can conclude that the condensational growth in the model produces trajectories in similar directions to what we observed in the paper.

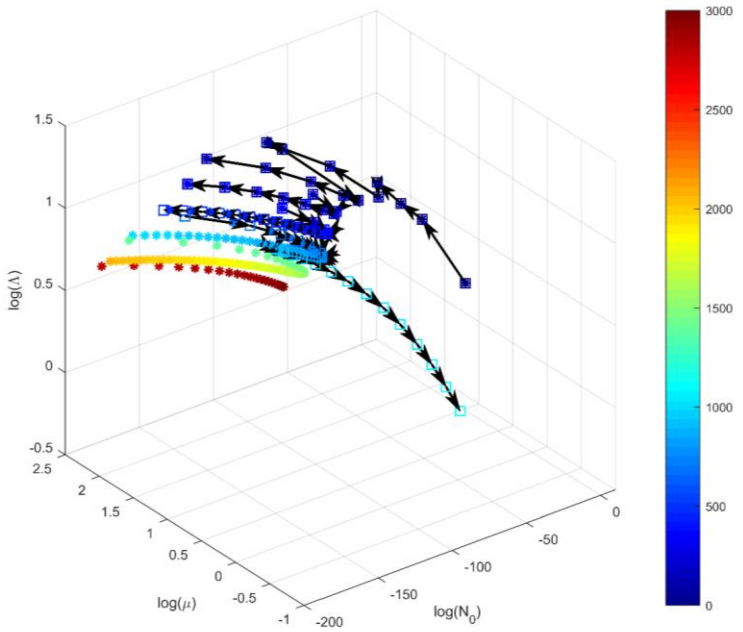

Figure R1: Gamma phase-space for both CG and C2G runs. The "*" markers are relative to the CG run, while squares represent the C2G run. Arrows represent the displacement vector between each 20-s point, which is related to the respective pseudo-force. Colors represent altitude above cloud base in m.

Figure R2 shows the same points of Figure R1, but colored according to D_{eff}. Additionally, we show lines of constant D_{eff} along a surface (not shown) of N_d = 250 cm^{-3} similarly to Figure 10 in the paper. The lines start at 5 µm in the top and grow in 5 µm intervals up to 50 µm in the bottom line. When comparing the trajectories with the D_{eff} lines, it is possible to see where the droplets are growing faster. For instance,

the condensational growth close to cloud base is very effective (because the droplets are smaller) and the trajectory tend to cross the D_{eff} lines. However, when droplets reach $D_{eff} \approx 25$ µm, the trajectories get almost parallel to the lines, showing slower growth. On the other hand, the collisional growth accelerates with increasing D_{eff}. This is expected from theory, but it is interesting to quantify its effects on the spherical coordinates of the displacement vectors – Figure R3.

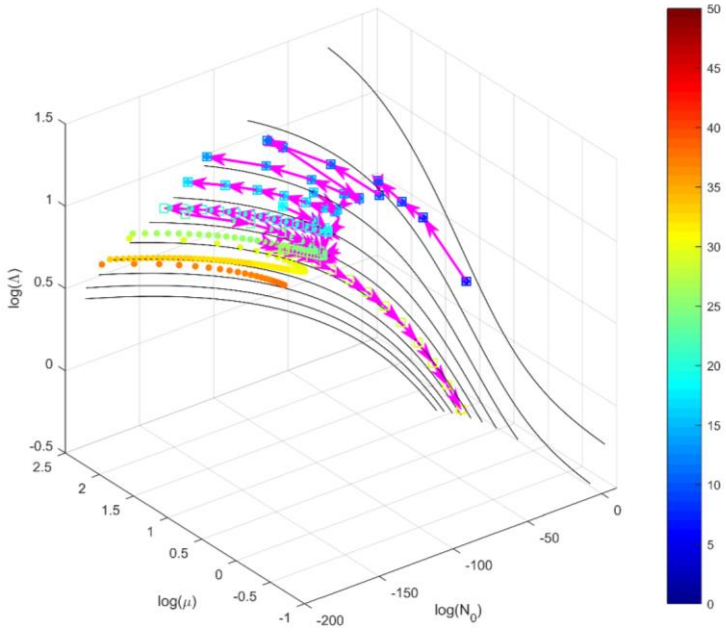

Figure R2: similar to Figure R1, but colored according to D_{eff}. The lines shown are lines of constant D_{eff} along a surface of $N_d = 250$ cm^{-3} as in Figure 10 in the paper, going from 5 µm (top line) to 50 µm (bottom line) – 5 µm intervals.

Figure R3 shows the spherical coordinates of the vectors in Figures R1 and R2. θ is the azimuth angle measured in the plane log(N_0) x log(µ), being 0 at the log(N_0) axis and growing counter-clockwise. φ is the elevation angle, measured from the plane log(N_0) x log(µ) to the log(Λ) axis. The size of the vectors

is measured by r. In Figure R3 we excluded the points in the downward part of the "zig-zag" mentioned above. Non-filled circles in Figure R3 represent condensational growth alone, while filled markers represent collision-coalescence (colors are altitude above cloud base in m). It is possible to note that the elevation angle φ is slightly positive for the condensational growth, decaying with D_{eff}. The average value of this angle is 0.26 °. It has small values mainly because of the bigger values of $\log(N_0)$ as compared to $\log(\Lambda)$. Nonetheless, the most important feature is its sign transition from condensational to collisional growth. On the latter, the angle seems to grow linearly with D_{eff} (except for the last point) as the process intensifies – averaged value of -4.23 °. Overall, this angle is related to the DSD curvature trend – positive when the curvature is shrinking (condensational growth) and negative when the curvature is increasing (collisional growth).

The azimuth angle θ defines how N_0 and μ evolve along the trajectory. For the condensational growth, this angle averages 179.6 °, meaning growing $\log(\mu)$ and shrinking $\log(N_0)$. On the other hand, this angle averages -13.7 ° for collisional growth and results in the opposite trend for the parameters. Both observations are in line with what we observed in the paper – now there is at least some quantification of the angles. Note that the angles most likely have different values in our observations given the differences in the values of the Gamma parameters. However, their sign, and therefore the direction of the motion in the space, is the same between our model calculations and the observations shown in the paper. Finally, we can note that r tends to decrease as the condensation rates decay, but it does not increase as the collisional growth intensifies. However, the acceleration of the collisional growth is reflected in φ and θ – both decrease, resulting in a trajectory that crosses the D_{eff} lines in Figure R2.

Overall, the modeling results presented here clearly indicate that the patterns observed in the Gamma phase space in the paper are indeed related to the condensation and collision-coalescence processes. The relation between both processes and the evolution of the Gamma parameters are consistent between the Lagrangian simulation and the observations. The natural next step would be to calculate the speeds and accelerations (and therefore the actual pseudo-forces), but this will not be addressed in this introduction paper. The actual implementation of the concepts presented here would need further work that is beyond the scope of the present study. A study is underway using different parametrizations, aerosol properties and environmental properties.

We added three new paragraphs to Section 2.3 commenting on the Lagrangian model results and detailed it a little more in the supplement (with the figures/text shown here for the readers).

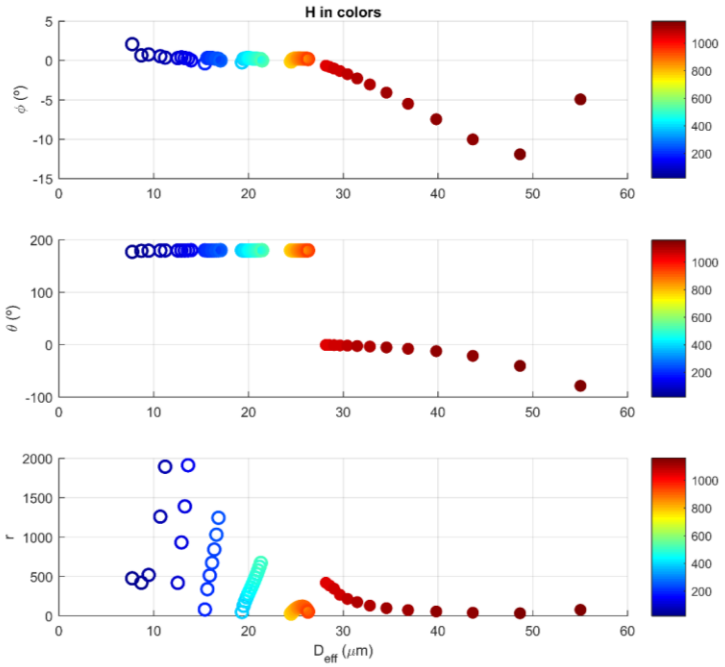

Figure R3: spherical coordinates of the displacement vectors shown in Figures R1 and R2. θ is the azimuth angle in the log(N_0) x log(μ) plane, growing counter-clockwise (is 0 at the log(N_0) axis). φ is the elevation angle from the log(N_0) x log(μ) towards the log(Λ) axis and r is the size of the vectors. The colors represent altitude above cloud base in m.

3. **(Comment)** Secondly, gamma functions often provide good mathematical fits to drop size distributions, but attempting to understand cloud processes using the fit coefficients is fraught with difficulty, which I don't think is addressed sufficiently in this manuscript. Gamma function coefficients can vary

substantially depending on the fit method used, the size range over which the fit is made, and the suitability of the underlying size distribution shape to be fit with a gamma. Many of these issues were addressed in the recent publication by McFarquhar et al. (JAS 2014). Using different fitting methods they found that the N0 coefficient, for example, can vary by many orders of magnitude, even when the same moments (1, 2, and 6) are used to make the fit. Using a different set of moments, like the 0th, 2nd, and 3rd used in this manuscript would likely result in even larger changes. Furthermore, the coefficients N0 and mu are inextricably linked, with N0 having the units of mˆ(-4-mu). So as mu changes, N0 will respond mathematically, even though such a change may not represent a physical process.

3. **(Answer)** The Gamma function and its parameters are indeed complex to use in practical applications. Additionally, the N_0, μ, and Λ parameters can sometimes seem as abstract numbers that are mathematically loosely defined. In other words, those parameters can have extreme behaviors depending on the way you choose to calculate them. However, their values and, perhaps most importantly, their interdependence is singular in each methodology. For instance, we could have different values for the Gamma parameters shown in the paper and the spherical coordinates shown in Figure R3 if we were to use, say, moments 3, 4, and 6 for the fit. If we were to compare between the two methodologies, it wouldn't be a fair comparison because their internal functioning (i.e. their parameter space) is different. Fits that use higher-order moments have stronger weights for bigger droplets, affecting the parameters values and their phase space. What we can do is to fix in a particular methodology and make the pattern analysis inside its particular phase space. We specifically chose to use moments 0, 2, and 3 in order to obtain a parameter space that is similar to what a bulk model should be able to reproduce. With regards to the moment method, we believe this is the best approach given that it precisely reproduces at least 2 moments predicted by bulk models (e.g. droplet number concentration and liquid water mixing ratio).

When the methodology is fixed, it doesn't really matter if, for instance, N_0 covers several orders of magnitude. In our modeling calculations N_0 went from $\sim 10^{-150}$ to $\sim 10^{1}$, but all those values are inside the phase space and can be expected when the DSDs fit certain criteria. We noted that N_0 reach such low values for narrower DSDs, like the ones that appear after long periods of (exclusively) condensational growth. Therefore, the theoretical phase space allows for such wide variability. The observations, on the other

hand, will of course cover a much more limited volume in the phase space. The idea is that both theoretical and observed phase spaces operate under the same underlying "laws" – at least considering only condensation and collision-coalescence growth, the model should be expanded to encompass other processes.

Regarding the linkage between N_0 and μ: as you correctly pointed out, those parameters are mathematically linked by definition. In fact, all three parameters are correlated in one way or another. When you go back to the equations used to obtain the parameters, this is very clear: first you obtain μ as a function of a dimensionless ratio between the moments, then you obtain Λ from μ, and finally N_0 from both of them. The relation between the Gamma parameters, modulated by the three moments, is a key aspect that generates the trajectories observed. If the parameters were completely independent, there wouldn't be trajectories in the phase space. There would probably be "clusters" of points for various types of DSDs. Our methodology aims to take advantage of this relationship in order to help on pattern recognition. It follows that the phase space is non-orthogonal, where it can "shrink" or "inflate" depending on the region of analysis. This is possibly one of the difficulties in applying this method to models, because the mathematic deductions are not straightforward. However, the ability to describe the microphysical evolution in this space opens new possibilities for DSD modeling, potentially improving subsequent calculations such as evaporation, sedimentation, etc.

I understand that the relationship between μ and N_0 is mathematical, but I would like to point out that it also makes physical sense. Take Equation 9 from the paper:

$$\varepsilon = \frac{\sigma}{D_g} = \frac{1}{\sqrt{\mu + 1}}$$

This equation states that the relative dispersion (or DSD width) can be calculated directly from μ. When μ increases, the DSD gets narrower. In that case, the left tail of the DSD gets closer to the maximum concentration diameter. Therefore, the intercept has to be lower and N_0 also shrinks. If you consider condensational growth, the situation is the same – see figures here and in the paper. Therefore, the linkage between N_0 and μ also have association to physical processes. When we look at the collision-coalescence growth, the opposite happens - μ decreases causing N_0 to increase.

4. **(Comment)** A more effective method may be to plot the moments themselves in 3D space rather than first fitting them to a gamma function. The moments are more easily linked to known microphysical processes, and if they are computed directly from the distributions do not suffer from the complications of poor fitting. The moments can always be computed from modeled DSDs as well, which would the avoid the further complications introduced when models use restricted gamma parameter spaces. At the very least, I think the authors should investigate the sensitivity of the observed phase-space patterns to different gamma fitting methods, and more clearly identify the source and interpretation of the F_cd and F_cl pseudo-forces.

4. **(Answer)** We believe that plotting the moments in a 3D space would be very similar to plotting the Gamma parameters. The moments are also not independent, thus resulting in a similar non-orthogonal space. However, the linkage between the moments-space and the underlying DSD is non-trivial. You would need to apply transformations to obtain the respective DSDs. Therefore, we believe the Gamma phase-space is more suitable in order to be portable for other applications. Also, as commented above, some calculations explicitly need the DSD parameters.

Regarding other methods to fit the DSDs, we tested a new fit based on moments of order 3, 4, and 6 (M346). Here we reproduce Figures R1-3 with this new approach (Figures R4-6). For this case, we had to limit the fittings to $D < 150$ μm because of the stronger weight to bigger droplets that caused negative values of μ. Note that the patterns in the phase-space are very similar to the previous case (M023). Averaged values for θ and φ are 179.5 ° and 0.35 ° for condensation and -19.4 ° and -4.0 ° for collision-coalescence, respectively.

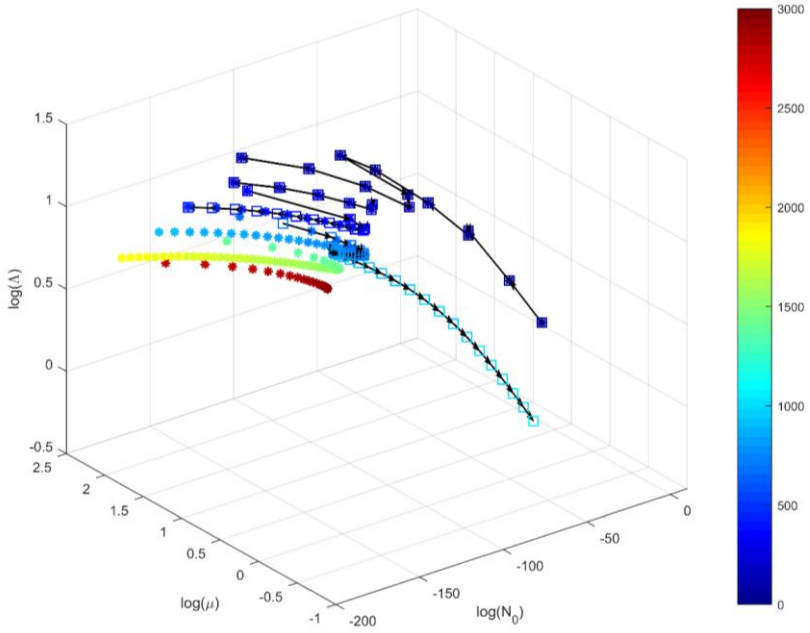

Figure R4: same as Figure R1, but for M346.

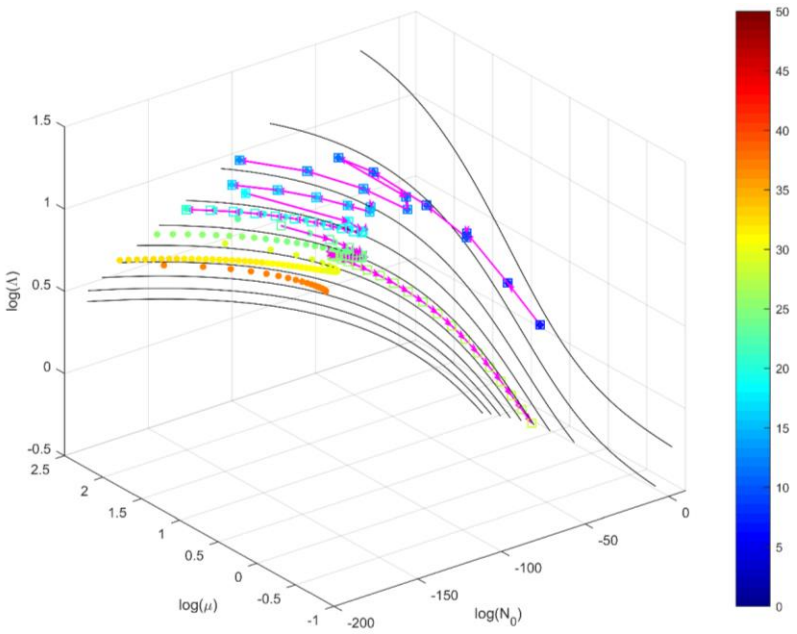

Figure R5: same as Figure R2, but for M346.

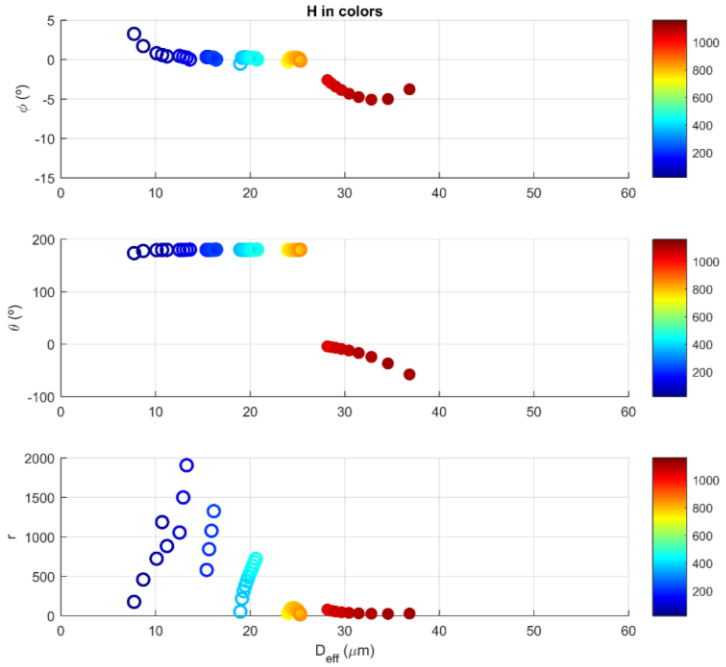

Figure R6: same as Figure R3, but for M346.

Specific comments:

1. **(Comment)** Section 2.2: How were DSD shapes that are not well fit by a gamma function handled in the analysis (e.g. bimodal or skewed distributions)?

1. **(Answer)** No special routine was applied to bimodal or skewed distributions. The idea is to produce the phase-space of the observations as is (except for the filter to remove residual DSDs) within the limitations of the Gamma fit.

2. **(Comment)** Section 2.3: The introduction of the F_cd and F_cl pseudo-forces seem incomplete and leaves many unanswered question, such as: How were they determined, i.e. can they be presented mathematically? Do they completely describe the total force F? Are they orthogonal, if not, in which direction in the phase space does each force point?

2. **(Answer)** Please refer to our answer to your major comments and the new paragraphs in Section 2.3.

3. **(Comment)** Figures 3,5,6,7, and 8: It is difficult to determine where the lines and points are in 3-D space. A projection of the fit lines onto the X, Y, and Z planes would greatly help with the visualization.

3. **(Answer)** We left Figure 3 as is for simplicity, but added the requested projections to the other figures.

4. **(Comment)** Section 2.3: Given the sensitivity of N0 to the mu parameter, the speculations regarding N_0 would be much more convincing if N_d (or 0th moment) were used instead.

4. **(Answer)** Our affirmations about N_0 were not speculations, but based on our measurements – note that the trajectories shown in Figures 5-8 point out to the patterns commented in Section 2.3. The new model calculations also corroborate our affirmations.

5. **(Comment)** Section 3.2: The manuscript states that measurements were taken 'close to cloud top', but more information is needed about the placement of the measurements in the cloud. Was the aircraft making multiple passes to a fixed location, or attempting to intercept the same visual position in the cloud on mulitple passes? How long did the aircraft pattern take relative to the lifetime of the cloud, and at what point the life cycle of the cloud were the measurements taken?

5. **(Answer)** We added the following sentences to Section 2.1 to clarify the flight strategy: "The latter step was deployed as follows. After the cloud base penetration, the aircraft performed several penetrations

in vertical steps of several hundred meters. In each step, the aircraft penetrated the cloud tops available, thus avoiding precipitation from above. In this way, different clouds can be penetrated in the same altitude level, but the vertical steps followed the growing cumuli field overall".

6. **(Comment)** Section 3.3: How were the clean and polluted clouds determined? Were the flight patterns and environmental conditions for each of these clouds comparable?

6. **(Answer)** The clean and polluted clouds were determined based on the measurements shown in Table 1 – i.e. the aerosol concentrations. All flight patterns followed the steps we described in Section 2.1 and we also show them in the map in Figure 1. The environmental conditions are discussed in Figure 4 and Table 1.

Authors response to Anonymous Referee #3

Major comments:

(Comment) This paper uses fits of measured cloud droplet size distributions (DSDs) in gamma phase space to investigate warm-phase microphysical cloud properties and the role of "pseudo-forces" in affecting the evolution of the gamma parameters and the DSDs. Overall, I found the description of a unique set of data interesting and formative, and hence believe that the paper is worthy of publication. However, there are some issues that should be addressed in order to improve the presentation before the paper is published as discussed below.

(Answer) We would like to thank Anonymous Referee #3 for the invaluable comments. Below we address them individually as best we can.

1. **(Comment)** The authors segregate the flights that are flown into the different regions of the Amazon where they are flown. Although changes in surface conditions are no doubt important for affecting the

cloud properties, meteorological conditions can also have an important impact on cloud properties. Some comments about this should be added to the manuscript and some analysis of the meteorology on the different days should be added to see if such differences can also explain some of the variation in cloud properties. I think attributing much of the changes to aerosols is not fully justified until the meteorological context is further explored.

1. **(Answer)** The meteorological context is clearly determinant for cloud formation over the Amazon or over any other region. We address this issue in two steps in the paper. Firstly, we show satellite images in Figure 2, clearly indicating the predominance of cumuli fields for all flights chosen. Flight AC07 deviates a little from this pattern, where deeper convection was observed. However, the aircraft pilot usually avoided penetrating deeper convection for safety reasons (at least in the lower levels). Therefore, even if there was deeper convection in the region, the aircraft actually penetrated the growing convective elements around it. Additionally, we show temperature and humidity profiles in Figure 4. Those profiles show that, even though the cumuli fields are relatively similar, there are some thermodynamic differences. Clouds over the Southern Amazon were subject to drier and warmer air, justifying their higher cloud base altitude. We do not believe that those differences would significantly impact the characteristics of the warm-phase DSDs. They may impact the overall lifecycle of the clouds and precipitation, but the microphysics in the lower parts of the clouds likely depend on factors such as updraft speed and, most importantly, aerosol concentration and size distribution. The effects of thermodynamics and aerosol properties on cloud microphysics were studied in a precedent paper (same special issues - https://doi.org/10.5194/acp-17-10037-2017).

2. **(Comment)** I was a bit surprised on page 6 where the authors described that they were focusing on the CDP measurements where D < 50 micrometers. It would seem to me to be quite important to also examine the drizzle sized drops measured by the CIP, as when drizzle was present it would seem to be very important to account for that in the analysis. How are flights handled when there was some precipitation-sized drops? Were these larger drops incorporated into the analysis of simply ignored? Further, for Eq.

(2) to Eq. (4) should the incomplete gamma function rather than the gamma function be used to account for the fact that not the complete size range of particles were measured?

2. **(Answer)** In this study, we are really interested in analyzing cloud droplet physics rather than drizzle/precipitation physics. Those are rather different. For instance, the condensational pseudo force is mostly insignificant for precipitation-sized liquid droplets. We indeed removed the drizzle/precipitation droplets from CIP for the Gamma fit, similarly to what models do. Models separate cloud and precipitation DSDs, that can be combined if need be. Another reason is that droplets with D > 50 μm were relatively infrequent in our measurements. In the warm phase, T > 0 °C, the number of data with $LWC_{D>50}$ > 0.1 g m^{-3} is only 8% of the cases where $LWC_{D<50}$ > 0.1 g m^{-3} (i.e. only a small portion of the data contained significant amounts of drizzle/precipitation). We added the following sentences to the second paragraph in Section 2.2: "The intent is to focus on cloud droplet growth processes and bringing the analysis closer to modeling scenarios. Additionally, the percentage of data with significant liquid water content (LWC) for D > 50 μm is relatively small. The number of data with $LWC_{D>50}$ > 0.1 g m^{-3} is only 8% of the number of DSDs with $LWC_{D<50}$ > 0.1 g m^{-3}".

Regarding the incomplete Gamma function, we reproduce our answer #4 for Anonymous Referee #4: "While we agree that the incomplete Gamma distribution would fit better the measurements, its use would result in other issues. As one of the main interests of the paper is to study the theoretical Gamma phase-space and its applicability to cloud modeling in the future, the use of the incomplete Gamma would not be ideal. In a modeling scenario, you don't have the observed DSD and therefore have no way of finding the truncation diameters. Additionally, the use of the incomplete Gamma distribution might add artificial patterns to the phase-space that are due to the truncation and not to physical processes".

3. **(Comment)** I think some more comments on the quality of the microphysical measurements are needed. How did the CAS and CDP probes compare? What are the estimated uncertainties in the size distributions? How did the LWC integrated from the CAS or CDP compare with bulk measurements from a hot-wire probe, which I am assuming were made. I am assuming that fits were only done to the liquid

distributions, or do you use all the distributions? This should be clearly stated when discussing the phase partitioning at the bottom of page 8.

3. **(Answer)** The instruments uncertainty, as well as their inter-comparison, is thoroughly analyzed in Braga et al. (2017) – same special issue (ACRIDICON-CHUVA). We updated the text with this reference (see second paragraph in Section 2.2). The fits were made to all measurements, irrespective of the NIXE-CAPS classification. However, this should not result in problems for our analysis given that the focus of the fits was primarily in the warm phase. Note that we do not draw any conclusions regarding the fits for regions above the transition between warm and mixed layers. We added the following sentence at the end on the NIXE-CAPS paragraph in page 8 to reflect this comment: "The NIXE-CAPS classification is a separate analysis and will not be considered as a filter to apply the Gamma fits to the CDP measurements. The CDP data fits are primarily focused on the warm phase and the transition to the mixed layer, where liquid droplets predominate".

4. **(Comment)** The implicit basis of the analysis presented in the Gamma phase space is that one is dealing with a Lagrangian case. But, inevitably, with any sort of microphysical measurements different samples of particle populations are being sampled. Further, there can be mixing and dynamic motions in clouds that would affect how the DSDs vary in the gamma phase space. Is there any way of representing these mixing processes on the diagram? I also think the action of the pseudo-forces and the impact of condensational growth and collision-coalescence could be better illustrated on the diagram. Can you show an example size distribution (it can be a theoretical rather than observed distribution if it is easier) and show how the size distribution would change due to simple model calculations of either condensational or collision-coalescence growth. Then, illustrate the location of all 3 DSDs (original, one undergoing condensational growth, and one undergoing collision-coalescence growth) on the gamma phase space and it will be easier for the reader to appreciate how these forces are represented on the diagram. Such simple theoretical/modeling calculations may also help you assess how the DSD characteristics are being affect by homogeneous/inhomogeneous mixing (discussion at top of page 12).

4. **(Answer)** As you correctly pointed out, it is impossible to produce Lagrangian trajectories based on aircraft microphysical measurements. Therefore, we have to make some assumptions to constrain our method. The flight patterns were specifically chosen in order to follow growing convective elements, where the aircraft penetrated the tops of the clouds. In this way, we both avoided precipitation from above and also tightened the relationship between the altitude of the measurements and the lifecycle of the clouds. We do not presume to claim that this guarantees that our trajectories are Lagrangian. In fact, when it comes to the observations, we never mention it. We just use the altitude of the measurements as a proxy for cloud evolution, meaning that higher measurements present "older" droplets. We believe this is rather reasonable and is also common place in microphysical studies. The confusion might come from the way we described the theory of the Gamma phase space in Section 2.3. In this idealized scenario, we can think of Lagrangian trajectories in order to facilitate the comprehension of the processes that affect DSD evolution. Now the link between the observations and the Lagrangian trajectories, for instance, should be addressed by other means such as modeling. As the title of the paper says, we illustrate the microphysical processes observed in the Gamma phase space rather than attempt to implement it in any actual modeling tool. This is the natural next step, of course, which is already ongoing. We added the following sentence in the second paragraph of Section 2.1 to further detail the flight patterns and why they could be used as a proxy for cloud evolution: "The latter step was deployed as follows. After the cloud base penetration, the aircraft performed several penetrations in vertical steps of several hundred meters. In each step, the aircraft penetrated the cloud tops available, thus avoiding precipitation from above. In this way, different clouds can be penetrated in the same altitude level, but the vertical steps followed the growing cumuli field overall".

In order to compare the results in the paper to a Lagrangian case, we ran a simple model. Please refer to the answer #2 to Anonymous Referee #2. From those calculations, we were able to conclude two things. Firstly, that the qualitative results from the model agree well with our observations. Therefore, even though we could not produce Lagrangian observations, they agree with Lagrangian calculations. Secondly, we were able to test your suggestion regarding the actual calculations of the pseudo-forces (or at least displacements in the phase-space). We were able to confirm the overall directions of the pseudo-forces between the observations and the model, while also quantifying the displacements due to each

growth process. The details of the model run can be found in the mentioned answer #2 to Anonymous Referee #2. We also added three new paragraphs to Section 2.3 commenting on the Lagrangian results. Additionally, the answer to Anonymous Referee #2 were also compiled in a new supplement.

Regarding the effects of homogeneous or inhomogeneous mixing in the phase-space, we believe it is beyond the scope of this work – which is focused primarily on condensation and collision-coalescence. However, it shouldn't be hard to analyze the effects on the phase-space. Note that there is significant literature regarding the effects of mixing on the DSDs. Therefore, one suggestion would be to apply the knowledge we have to a Gamma DSD and study the displacements in the phase-space.

5. **(Comment)** I'm wondering if some different terminology could be used to refer to the different flights. Although referring to flight numbers (e.g., AC19, AC18, AC12, etc.) might be very informative for people who were involved in the field program, I continually had to refer back to the table to remember the regions in which the flights were conducted to help interpret the data. Can you refer to them as maybe AC1 (AC19 for Atlantic coast 1), RA1 and RA2 (AC09 and AC18) for remote Amazon, and AD1, AD2 and AD3 (for AC07, AC12, and AC13) so that it is more easy to remember the flights going through the manuscript. Or, maybe some other terminology would also work.

5. **(Answer)** Indeed, this would greatly facilitate reading the paper. We kept the ACXX nomenclature in Table 1 for consistency with the other special issue papers and added the new definitions as: 1) M1 (as in Maritime1 - AC1 might be confused with the ferry flight with the same nomenclature even though we don't mention it in our paper) for flight AC19; 2) RA1 and RA2 for AC09 and AC18 as you suggested; and 3) AD1, AD2, and AD3 also per your suggestion.

6. **(Comment)** With regards to the depiction of the DSDs in phase space, I would find it much easier is some 2-d cross sections were presented in addition to the 3-d volumes (it was hard to follow some of the discussion on the contrasts between clean and polluted trajectories). It is very hard to visualize how the different parameters are changing on these 3-d plots, so some 2-d cross sections would also offer some

supplementary information. Further, what are the uncertainties or range of possible values in the gamma parameters.

6. **(Answer)** Thank you for this suggestion, we added the requested cross sections and it is much better now. With regards to the data spread around the trajectories, it can already be observed in Figures 5-7.

Minor Comments:

1. **(Comment)** Page 2, Line 20: I was surprised to see that the undisturbed portions of the rainforest are said to have homogeneous surface properties: compared to oceanic surfaces surely the nature of the forest is somewhat inhomogeneous? On page 5 (lines 20-25), the authors talk about differences in surface and thermodynamic conditions on more of the disturbed areas of the Amazon, so I found that this comment was a bit misleading.

1. **(Answer)** Surface conditions over the forest is indeed less homogeneous than over the ocean. The intended meaning is to say that it is more homogeneous than urbanized regions. The sentenced was changed to reflect this: "…Given the relative homogeneity of the surface (as compared to urbanized regions) and the pristine air over undisturbed portions of the rainforest…".

2. **(Comment)** Page 3, Line 1: Typically the term ice nucleating particles (INPs) rather than ice nuclei (IN) now. See Vali (2015).

2. **(Answer)** Agree, thanks.

3. **(Comment)** Page 4, line 9: Unless specific numeric values are quoted, the parameters of the gamma function (or any parameter in general) do not have units associated with them. They could be given in any unit with an appropriate conversion being made. Recommend removing the units in parenthesis.

3. **(Answer)** Added a clarification explaining that the units given are the ones to be considered in this study.

4. **(Comment)** Page 5, line 23: if the convective clouds were growing, how could you ensure that the third stage was always flown through the growing tops? It would seem that different altitudes below cloud top might have been sampled for the different population of clouds.

4. **(Answer)** The aircraft performed several steps in altitude and in each level the pilot looked for cloud tops available for penetration. There may be some differences regarding the distance to the cloud top, but the overall intent was to minimize precipitation falling from above as much as possible.

5. **(Comment)** Page 7, Eq. (7). I don't think this equation is correct (the factor of 10^-9). Any equation must be unit-independent. Constants for conversions between specific unit sets hence don't belong in equations as those factors will automatically appear when converting between the different units of the variables.

5. **(Answer)** We are sticking to the units we actually used. We provide them right after the equations, therefore it is easier for the reader to understand directly what we did. Added the following sentence before the equations for clarification: "In the units considered here, the equations are given by:".

6. **(Comment)** Page 8, line 4: If the fact epsilon obtained by the gamma parameters does not match those from the DSDs suggest that the gamma distribution does not give a good fit to the DSD?

6. **(Answer)** We mention that the Gamma-epsilon and the Observed-epsilon are tightly linked by eps_gamma = 0.95*eps_obs (R^2 = 0.93). Therefore, it is safe to say that the observed epsilon is well represented by the Gamma fit. The Gamma DSD is only slightly narrower (angular coefficient of 0.95). Changed the sentence to: "The relative dispersion of the Gamma DSD may differ from the observations, given the differences between the parameterized and observed DSDs. However, our measurements show

that the Gamma and observed ε are closely related by $\varepsilon_{Gamma} = 0.95\varepsilon_{Observed}$ (R^2 = 0.93), showing that the Gamma DSDs are slightly narrower on average" for clarification.

7. **(Comment)** Page 9, line 12: Can you use a different word rather than "phase transitions?" there is some confuse about whether you are talking about phase space or the phase (liquid, mixed or ice) of the cloud particles.

7. **(Answer)** Changed to phase-state transition.

8. **(Comment)** Page 11, line 16: "from drier air", can you list the humidities in Table 1?

8. **(Answer)** The humidity for the different regions is shown in Figure 4.

9. **(Comment)** Page 11, line 23: Do you mean average RH? Clouds do not form in an environment where the relative humidity at their location is between 60% and 90%. Can you also give some indication of the thickness of the different cloud layers?

9. **(Answer)** Added "surrounding environment" instead of only "environment" for clarification. This is the air around the clouds and not within them. It is hard to provide cloud thickness because they are growing as the airplane ascends. However, they can reach altitudes up to 15 km approximately.

10. **(Comment)** Page 12, lines 13-14: How do you know the observations were obtained close to cloud top? Unless you have remote sensing data or some ascents out of cloud, is it conceivable the particular cloud you were sampling extended to a higher height?

10. **(Answer)** As explained previously, we can be relatively sure that the aircraft penetrated the cloud top by the flight pattern planning. The pilot looked for cloud tops in each flight level.

11. **(Comment)** Page 13, line 1: What is classified as a significant difference? Was some sort of statistical test applied?

11. **(Answer)** Sentence changed to "At first glance, it is possible to see stronger differences between the trajectories in the different regions, while internal variations are much weaker".

12. **(Comment)** Page 14, line 12: What statistical test was applied to know that the res

12. **(Answer)** The text of this comment is cutout, so no changes were applied.

Authors response to Anonymous Referee #4

Major comments:

1. **(Comment)** This paper used in-situ data from six flights collected during the ACRIDICON-CHUVA field campaign to explore the linkage between gamma distribution parameter phase space and underlying microphysical processes. Three different environmental conditions, the Atlantic Coast, the remote Amazon, and the Arc of Deforestation were studied, and the differences in the underlying microphysical processes among these regions were compared. The paper fits into the scope of ACP and is generally well written, however, the approach used in this study has severe scientific flaws. Therefore, this paper needs to be revised considerably before it can be published in ACP.

1. **(Answer)** We would like to thank Anonymous Referee #4 for the invaluable comments. Please find in this document our detailed answers.

2. **(Comment)** Page 5, Line 15-18. Are there only six flights during the whole field campaign focusing on clouds? If not, why other flights are not used? Especially for Atlantic Coast, there is just one flight used.

2. **(Answer)** Yes, there were other flights that were partially dedicated to probe clouds. However, our specific focus on individual trajectories in this paper meant that we could exchange increased statistics for specialized analysis. The reasoning behind our flight selection was mostly due to the aerosol characteristics below clouds. All flights chosen presented relatively uniform aerosol number concentrations below clouds, therefore avoiding mixture of cleaner and more polluted clouds. On the other cloud profiling flights, we noted variations of the aerosol number concentrations, which would make the analysis much more difficult. By focusing on the selected flights, we were sure that each flight contained almost exclusively the same type of clouds in terms of aerosol conditions. The following sentence was added to the first paragraph in Section 2.1 for clarification: "There were other flights with cloud penetrations, but they are not considered in this study because of higher aerosol variability below clouds. The flights chosen for analysis presented relatively low aerosol variability, meaning that the clouds probed in the same flight were likely subject to similar aerosol conditions".

There was only one flight over the ocean, so we couldn't increase its statistics on the paper.

3. **(Comment)** Page 6, Line 22-24: Why PSDs from CIPgs is not used? Only using CDP to create PSDs with D < 50 um will miss out lots of water mass, therefore the third moment used for fitting will be much less.

3. **(Answer)** Our main interest in this study is on the Gamma trajectories of the cloud DSDs. We don't use CIPgs data because we consider them as drizzle/precipitation DSDs, therefore out of the scope of this study. Besides, there were relatively few DSDs for D > 50 µm. As we explained in our answer #2 to Anonymous Referee #3: "In the warm phase, T > 0 °C, the number of data with $LWC_{D>50} > 0.1$ g m^{-3} is only 8% of the cases where $LWC_{D<50} > 0.1$ g m^{-3} (i.e. only a small portion of the data contained significant amounts of drizzle/precipitation)".

4. **(Comment)** Page 7, Line 3-14: Incomplete gamma distribution should be used here since only a limited range of particle size is used for fitting. I believe this is the reason why fitted Gamma DSDs are narrower (Page 8, Line 1-4).

4. **(Answer)** While we agree that the incomplete Gamma distribution would fit better the measurements, its use would result in other issues. As one of the main interests of the paper is to study the theoretical Gamma phase-space and its applicability to models in the future, the use of the incomplete Gamma would not be ideal. In a modeling scenario, you don't have the observed DSD and therefore have no way of finding the truncation diameters. Additionally, the use of the incomplete Gamma distribution might add artificial patterns to the phase-space that are due to the truncation and not to physical processes. This point was clarified in the text right before Equation 2 with the following sentence: "The complete Gamma function is used to be consistent with modeling scenarios, where the Gamma parameters are calculated by:".

5. **(Comment)** Section 2.3. I have four major concerns for this method, and will elaborate them in next four points. As stated in Page 9, Line 9, this approach is suitable for the study of the same particle population, which is under Lagrangian framework. Therefore, aircraft dataset at different levels sampling different particle population cannot be used to track the change of cloud PSD gamma parameters, since they are not the same particle population. In addition, the PSDs at the same level are not the same and exhibit large variations. So, the best use of this technique will be for the parcel model if the authors can address the following three comments.

5. **(Answer)** Indeed, this is a valid concern that is also shared by the other reviewers. Here we reproduce our answer #4 to Anonymous Referee #3:

"As you correctly pointed out, it is impossible to produce Lagrangian trajectories based on aircraft microphysical measurements. Therefore, we have to make some assumptions to constrain our method. The flight patterns were specifically chosen in order to follow growing convective elements, where the aircraft penetrated the tops of the clouds. In this way, we both avoided precipitation from above and also tightened the relationship between the altitude of the measurements and the lifecycle of the clouds. We do not presume to claim that this guarantees that our trajectories are Lagrangian. In fact, when it comes to the observations, we never mention it. We just use the altitude of the measurements as a proxy for cloud

evolution, meaning that higher measurements present "older" droplets. We believe this is rather reasonable and is also common place in microphysical studies. The confusion might come from the way we described the theory of the Gamma phase space in Section 2.3. In this idealized scenario, we can think of Lagrangian trajectories in order to facilitate the comprehension of the processes that affect DSD evolution. Now the link between the observations and the Lagrangian trajectories, for instance, should be addressed by other means such as modeling. As the title of the paper says, we illustrate the microphysical processes observed in the Gamma phase space rather than attempt to implement it in any actual modeling tool. This is the natural next step, of course, which is already ongoing. We added the following sentence in the second paragraph of Section 2.1 to further detail the flight patterns and why they could be used as a proxy for cloud evolution: "The latter step was deployed as follows. After the cloud base penetration, the aircraft performed several penetrations in vertical steps of several hundred meters. In each step, the aircraft penetrated the cloud tops available, thus avoiding precipitation from above. In this way, different clouds can be penetrated in the same altitude level, but the vertical steps followed the growing cumuli field overall".

In order to compare the results in the paper to a Lagrangian case, we ran a simple model. Please refer to the answer #2 to Anonymous Referee #2. From those calculations, we were able to conclude two things. Firstly, that the qualitative results from the model agree well with our observations. Therefore, even though we could not produce Lagrangian observations, they agree with Lagrangian calculations. Secondly, we were able to test your suggestion regarding the actual calculations of the pseudo-forces (or at least displacements in the phase-space). We were able to confirm the overall directions of the pseudo-forces between the observations and the model, while also quantifying the displacements due to each growth process. The details of the model run can be found in the mentioned answer #2 to Anonymous Referee #2. We also added three new paragraphs to Section 2.3 commenting on the Lagrangian results. Additionally, the answer to Anonymous Referee #2 were also compiled in a new supplement".

6. **(Comment)** Even for the same PSD, there are large uncertainties as stated in Page 6, Line 27-Page 7, Line 1. McFarquhar et al. (2015) studied the uncertainties of counting statistics, and found that all the parameters within an ellipse in Gamma distribution parameter phase space are equally realizable. The

displacement of gamma distribution parameters could be just random values in the ellipse unless the ellipse of equally realizable solutions are defined for each PSDs.

6. **(Answer)** Yes, if we consider, for instance, the instrument uncertainty, we would end up with ellipsoids rather than points in the phase-space. However, given that the CDP uncertainty is about 10% (added this information to the second paragraph in Section 2.2), it is clear that the trajectories evolve beyond random movements in an ellipsoid. Let's consider, for the sake of this argument, that the instrument uncertainty is 10% for both the concentrations and the sizing of the droplets. In other words, let's consider that N_d, D_{eff}, and D_g all have 10% uncertainty. Now how that would translate to the phase-space?

We visualize the situation in Figure 10 of the paper. Each uncertainty mentioned could be associated to one of the three axes of the ellipsoids, which are either tangent or normal to the N_d surfaces in Figure 10. Consider that we are in the blue surface of Figure 10 (N_d = 10 cm^{-3}) and in the point where the blue trajectory crosses the upper black line where D_{eff} = 23 µm (they don't actually touch in the Figure 10, but let's consider they do). A 10% uncertainty in N_d would mean a normal axis to the blue surface (both towards and away from the green surface). The size of this axis would be very small in the figure, being 1/100 of the distance between the blue and the green surfaces. The uncertainty in D_{eff} would mean a tangent axis in the direction of the next black line (below), coincidentally of approximately the same size as the distance between the lines. If we consider that a 10% uncertainty in D_g translates to 10% error in ε, then we have the last axis – also tangent to the blue surface, but in the same direction as the D_{eff} line. The projection of the ellipsoid in the blue surface can be roughly represented by the purple curve in the figure below (note that the ellipsoid is very thin in the normal direction). Therefore, the trajectories cover wider regions than the ellipsoids dimensions and the trajectories approach is still valid. We added the following paragraph to the end of Section 2.3 to acknowledge the ellipsoid approach: "Another point to take into consideration are the ellipsoids discussed in McFarquhar et al. (2015). Basically, by considering the instrument and Gamma fitting uncertainties, it is possible to define volumes (with ellipsoid shapes) rather than individual points in the Gamma phase space. Inside each ellipsoid, all DSDs are equally realizable and therefore the movements within it have no particular physical meaning and are statistically the same. In this study, however, we estimate that the results evolve beyond individual ellipsoids and the patterns

are associated to physical processes. The results shown in the next sections will not consider the ellipsoid approach, but the points shown can be considered to be the central points of such volumes".

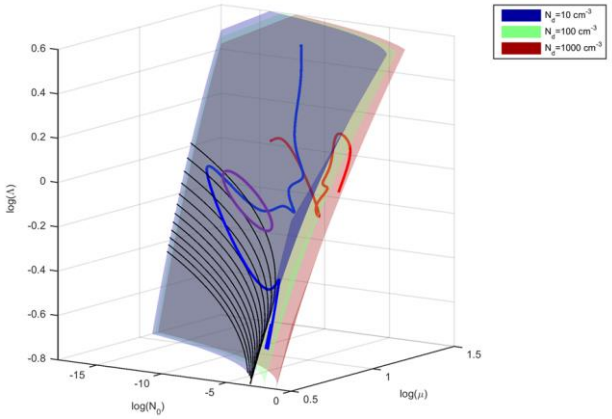

Figure R1: estimated size of the uncertainty ellipsoid in Figure 10 of the paper.

From this simple calculation, we conclude that the trajectories are likely to evolve beyond random movements in one ellipsoid. We won't carry this calculation over to the paper, however, because the trajectories can only be defined by points instead of volumes. In that sense, we can consider that the points in the trajectories are the central points of the ellipsoids. In the future, it would be interesting to study how the ellipsoids can be understood taking into account the underlying physics found in the phase-space.

7. **(Comment)** As for the "pseudo-forces", or microphysical processes which I prefer, this study decomposed it into two components: condensational growth and collision-coalescence growth. Due to the complex microphysical processes occurring in the clouds (as is discussed by the authors in Page 9, Line 21 – Page 10, Line 2), the evolutions of PSDs are very complex as some simulations using bin microphysics show. Simply relating a change of gamma distribution parameters to either condensational growth or collision-coalescence is not justified. Especially for any volume of air the aircraft sampled (or numerical models in Eulerian framework), the horizontal and vertical advection are very important.

7. **(Answer)** Yes, there are several other processes that affect the DSDs. However, we would argue that condensation and collision-coalescence are definitely the most determinant. Any model, however simple, should be able to reproduce those mechanisms in order to explain precipitation formation even though the other processes are also important. These other forces are also being studied in the phase space using different microphysical parameterizations and we hope to have further results soon. For this first introduction of the phase-space, we chose to focus on condensation and collision-coalescence in order to define the overall characteristics of the space and how we can analyze cloud DSDs evolution in it. The other processes can and should be analyzed on top of that basis.

Let's take the mixing processes as an example. There are several studies analyzing the effects of homogeneous or inhomogeneous mixing on the characteristics of the DSDs. Therefore, in principle, we should be able to estimate the effects of mixing on Gamma DSDs as well, which can be reproduced in the phase-space. This could explain some characteristics of the trajectories we observed, but we believe this kind of analysis is beyond the scope of our paper. We are considering this kind of analysis as the necessary next steps, which should involve other tools such as models.

That said, we ran a simple Lagrangian model with bin microphysics in order to check the patterns associated to condensation and collision-coalescence and if they match our observations. If they qualitatively agree, it means that our observations are capturing those microphysical processes. Please refer to our answer #2 to Anonymous Referee #2 where we detail the model runs and its results. Overall, we were able to confirm that the condensation and collision-coalescence processes induce displacements in the same directions that we inferred from the observations. Obviously, the quantitative results are different given that the model is relatively simple and does not consider several processes that affect our observations. But we believe this is a good indication that the Gamma phase-space methodology is consistent and that we should dedicate efforts to progressively include the other processes as well. In that regard, it would be interesting to analyze the Gamma phase-space in more complex models such as the LES-type.

8. **(Comment)** The directions and magnitudes of "condensational growth pseudo-force" and "collision-coalescence pseudo-force" are uncertain, which means that the influences of each individual microphysical processes on PSD evolutions are not studied clearly.

8. **(Answer)** Yes, we didn't explicitly quantify the pseudo-forces in this first introduction of the methodology. The main intent of this paper is to introduce the Gamma phase-space as a physical entity and illustrate microphysical processes in it. We believe the quantifications should be the focus of future implementations of the phase-space and is beyond the scope of the present work. However, the Lagrangian model runs we mentioned in the previous item can be considered as the first step in that direction. Note that the direction of the displacements is similar between the model and our observations. Therefore, the displacements in the observed trajectories can be at least partially explained by the processes considered in the model.

9. **(Comment)** The descriptions of "favors high value of mu while slightly increasing lambda" (Page 10, Line 4) and "lower values of lambda and mu, the former decreasing at a faster pace" (Page 10, Line 13-14) are not precise and not justified. The change of N_0 as described are wrong, since if condensational growth increase both μ and λ while keeping the same total number concentration, N_0 should also increase. In addition, if collision coalescence lower both μ and λ, and total number concentration of course, then N_0 should be also decreasing. Besides, I would say that evaporation "pseudo-force" acts the opposite way as "condensational growth pseudo-force" instead of "collision-coalescence pseudo-force" in this study. Anyway, the directions of these "pseudo-forces" are totally unknown, and the change of gamma distribution parameters could be any microphysical processes since relating the change of gamma distribution parameters (or equivalently PSD moments or bulk properties) to any single microphysical process is impossible.

9. **(Answer)** While our affirmations may not be precise, because it is pattern analysis instead of actual quantification, they are correct. Both our observations and the model calculations corroborate those affirmations. Please refer to our answer #2 to Anonymous Referee #2. In that document, we calculated the

elevation angle φ to be positive for the condensational growth, meaning increasing Λ. On the other hand, we calculated an average θ of 179.6 °. Because this angle is calculated from the log(N_0) axis, this value means growing μ and shrinking N_0 – second quadrant. For collision-coalescence, φ = -4.23 °, meaning decreasing Λ. The azimuth θ is -13.7 °, which is in the direction of growing N_0 and decreasing μ. We believe those quantifications are the first step at calculating the actual values of the pseudo-forces, but its implementation should be the focus of further studies in the future.

The "evaporation pseudo-force" is surely the opposite of the "condensational pseudo-force". But it is also true that the collision-coalescence pseudo-force acts in the opposite (overall) direction as the condensational pseudo-force.

Minor comments:

1. **(Comment)** Page 4, Line 24-25. This sentence needs to be elaborated.

1. **(Answer)** Changed to: "This process may produce artificial trajectories in the phase space by limiting the parameter variability".

2. **(Comment)** Figure 1. Add flight height and temperatures for each flight.

2. **(Answer)** We believe it would be hard to visualize the altitude and temperature in this figure. Instead, the requested properties can be seen in the other figures and tables in the paper.

3. **(Comment)** Page 5, Line 23 – Page 6, Line 10. The three regions used in section 3.2 should be introduced here clearly. Furthermore, the cloud characteristic for coastal region and remote Amazon should be described here, similar to what has been written for the Arc of Deforestation.

3. **(Answer)** Added the following sentence to the end of the second paragraph in this section: "Contrasting with the Arc of Deforestation, the region named Remote Amazon in this study has much lower background aerosol concentrations, producing cleaner clouds. Clouds over the Atlantic Ocean developed under cleaner conditions as compared to the continental counterparts, and also had lower cloud bases (Table 1)".

4. **(Comment)** Figure 5-8. The y and z axes (μ and λ) don't need to be taken logarithm for easy comparisons with previous studies. In addition, the projection of the 3D trajectories in N_0-μ, N_0-λ, μ-λ planes will make readers to follow easier.

4. **(Answer)** We analyzed the situation and decided that logarithmic axes were the easiest way to visualize the trajectories. The projections were added to the figures.

5. **(Comment)** Figure 5-8. Add raw PSDs with different colors showing different time, so the change of PSDs is clear to the readers. As shown in many previous studies (e.g., Heymsfield et al. 2013), the gamma distribution parameters can compensate with each other, therefore, the different points in the gamma distribution parameter phase space could mean the same PSD.

5. **(Answer)** We show observed and fitted DSDs in Figure 9. As far as the trajectories go, we did not observe any pair of similar DSDs with different Gamma parameters.

6. **(Comment)** Page 14, Line 23-27. Recommend removing these sentences. As stated in Major comment #7, the quantitative descriptions of these "pseudo-forces" are lacking. Besides, the method may just work for Lagrangian framework. I cannot see how this could be used for bulk microphysical schemes.

6. **(Answer)** We have shown that it is possible to produce quantifications of the processes using a simple Lagrangian model. Of course, the method should be refined to consider the many other aspects present in

clouds. We believe it is important to leave those affirmations in the paper, as they can be addressed by other researchers.

7. **(Comment)** Page 17, Line 10-21. According to Equation 9, this is similar to fix μ which is adopted in lots of numerical schemes. Actually, the small range of μ is due to its scale, and could mean large variations of PSDs.

7. **(Answer)** We left the second sentence in the last paragraph of Section 3.2 more open-ended: "If ε can be constrained in the model, it should be possible to obtain the full Gamma DSD – which is the point in the intersection curve that presents the given ε".

8. **(Comment)** Page 19, Line 11-12. The sentence that "The characteristics of the clouds warm layer. . .should have a determining role in the glaciation initiation". I would argue that the IN and the ice microphysics above are more important. The characteristic of IN between the remote Amazon and the Arc of Deforestation are not studied. The number concentration of ice particles above should also be analyzed, which may explain the differences in glaciation.

8. **(Answer)** In this sentence we refer to the glaciation initiation – imagining a cloud that is growing past the 0 °C and does not have an ice phase yet. In this scenario, the characteristics of the droplets that cross the 0 °C isotherm are definitely important to trigger (or not) the glaciation process.
Yes, it is unsure how the IN population changes with pollution, but previous studies suggest that most of the IN over the Amazon come from natural sources – either from the forest or from long range transport (Saharan dust).

Illustration of microphysical processes in Amazonian deep convective clouds in the Gamma phase space: Introduction and potential applications

Micael A. Cecchini[1,6], Luiz A. T. Machado[1], Manfred Wendisch[2], Anja Costa[3], Martina Krämer[3], Meinrat O. Andreae[4,5], Armin Afchine[3], Rachel I. Albrecht[6], Paulo Artaxo[7], Stephan Borrmann[4,8], Daniel Fütterer[9], Thomas Klimach[4], Christoph Mahnke[4,8], Scot T. Martin[10], Andreas Minikin[19,11], Sergej Molleker[8], Lianet H. Pardo[1], Christopher Pöhlker[4], Mira L. Pöhlker[4], Ulrich Pöschl[4], Daniel Rosenfeld[12], Bernadett Weinzierl[9,13,14]

[1]Centro de Previsão de Tempo e Estudos Climáticos, Instituto Nacional de Pesquisas Espaciais, Cachoeira Paulista, Brasil.
[2]Leipziger Institut für Meteorologie (LIM), Universität Leipzig, Stephanstr. 3, 04103 Leipzig, Deutschland.
[3]Forschungszentrum Jülich, Institut für Energie und Klimaforschung (IEK-7), Jülich, Germany.
[4]Biogeochemistry, Multiphase Chemistry, and Particle Chemistry Departments, Max Planck Institute for Chemistry, P.O. Box 3060, 55020, Mainz, Germany.
[5]Scripps Institution of Oceanography, University of California San Diego, La Jolla, CA 92037, USA.
[6]Departamento de Ciências Atmosféricas, Instituto de Astronomia, Geofísica e Ciências Atmosféricas (IAG), Universidade de São Paulo (USP), Brasil.
[7]Instituto de Física (IF), Universidade de São Paulo (USP), São Paulo, Brasil.
[8]Institut für Physik der Atmosphäre (IPA), Johannes Gutenberg-Universität, Mainz, Deutschland.
[9]Institut für Physik der Atmosphäre, Deutsches Zentrum für Luft- und Raumfahrt (DLR), Oberpfaffenhofen, 82234 Wessling, Deutschland.
[10]School of Engineering and Applied Sciences and Department of Earth and Planetary Sciences, Harvard University, Cambridge, Massachusetts, USA.
[11]Flugexperimente, Deutsches Zentrum für Luft- und Raumfahrt (DLR), Oberpfaffenhofen, Deutschland.
[12]Institute of Earth Sciences, The Hebrew University of Jerusalem, Israel.
[13]Faculty of Physics, University of Vienna, Boltzmanngasse 5, 1090 Wien, Austria.
[14]Ludwig-Maximilians-Universität, Meteorologisches Institut, München, Deutschland.

Correspondence to: M. A. Cecchini (micael.cecchini@gmail.com)

Abstract. The behavior of tropical clouds remains a major open scientific question, ~~given that the associated physics is not well~~resulting in poor ~~represented~~ representation by models. One challenge is to realistically reproduce cloud droplet size distributions (DSD) and their evolution over time and space. Many applications, not limited to models, use the Gamma function to represent DSDs. However, even though the statistical characteristics of the Gamma parameters have been widely studied, there is almost no study dedicated to understanding the phase space of this function and the associated physics. This phase space can be defined~~, which is given~~ by the three parameters that define the DSD intercept, shape, and curvature. Gamma phase space may provide a common framework for parameterizations and inter-comparisons.

Here, we introduce the phase-space approach and its characteristics, focusing on warm-phase microphysical cloud properties and the transition to the mixed-phase layer. We show that trajectories in this phase space can represent DSD evolution and can be related to growth processes. Condensational and collisional growth may be interpreted as pseudo-forces that induce displacements in opposite directions within the phase space. The actually observed movements in the phase space are a result of the combination of such pseudo-forces. Additionally, aerosol effects can be evaluated given their significant impact on DSDs. The DSDs associated with liquid droplets that favor cloud glaciation can be delimited in the phase space, which can help models to adequately predict the transition to the mixed phase. We also consider possible ways to constrain the DSD in two-moment bulk microphysics schemes, where the relative dispersion parameter of the DSD can play a significant role. Overall, the Gamma phase-space approach can be an invaluable tool for studying cloud microphysical evolution and can be readily applied in many scenarios that rely on Gamma DSDs.

1 Introduction

Tropical deep convective clouds (DCCs) constitute an important source of precipitation (Liu 2011) and they interact with atmospheric solar and terrestrial radiation, dynamical processes and the hydrological cycle (Arakawa 2004). Deep tropical convection is responsible for transporting energy upwards and thus sustaining the Hadley circulation that redistributes heat to higher latitudes (Riehl and Malkus 1958; Riehl and Simpson 1979; Fierro et al. 2009, 2012). Therefore, understanding the processes that impact the characteristics of tropical DCCs is crucial in order to comprehend and model the Earth's climate.

The DCCs over the Amazon are of particular interest. Given the relative homogeneity of the surface (as compared to urbanized regions) and the pristine air over undisturbed portions of the rainforest, Amazonian DCCs can have similar properties to maritime systems (Andreae et al. 2004). At the same time, their daily persistence and the considerable latent heat release have a noticeable impact on the South America climate by, for instance, maintaining the Bolivian High, which is a key component of the South American monsoon system (Zhou and Lau 1998; Vera et al. 2006).

Clouds and aerosol particles interact in a unique way in the Amazon. Low concentrations of natural aerosols derived from the forest are the major source of natural cloud condensation nuclei (CCN) and ice

nucleating particles~~i~~ (INPs) populations under undisturbed conditions (Pöschl et al., 2010; Prenni et al., 2009; Pöhlker et al., 2012, 2016). Other sources of aerosol particles over the Amazon include long range Saharan dust and sea salt transport, biomass burning (either naturally-occurring or human-induced) and urban pollution downwind from cities and settlements (Talbot et al., 1988,1990; Cecchini et al., 2016; Martin et al., 2010; Kuhn et al., 2010).

Human-emitted pollution can significantly alter cloud properties by enhancing CCN number concentrations (N_{CCN}). Since the work of Twomey (1974) analyzing the effects of enhanced N_{CCN} on cloud albedo, much attention has been given to aerosol-cloud-precipitation interactions. The effects of aerosol particles on warm-phase precipitation formation is fairly well understood, where enhanced CCN concentrations lead to the formation of more numerous but smaller droplets delaying the onset of rain (Albrecht 1989; Seifert and Beheng 2006; van den Heever et al. 2006; Rosenfeld et al. 2008). However, in mixed-phase clouds, the rain suppression by pollution can enhance ice formation leading to stronger updrafts and convective invigoration (Andreae et al. 2004; Khain et al. 2005; van den Heever et al. 2006; Fan et al. 2007; van den Heever and Cotton 2007; Lee et al. 2008; Rosenfeld et al. 2008; Koren et al. 2010; Li et al. 2012; Gonçalves et al., 2015). Aerosol effects on clouds have been reviewed by Tao et al. (2012), Rosenfeld et al. (2014), and Fan et al. (2016). By changing cloud properties, aerosol particles have an indirect impact on the thermodynamics of local cloud fields through, for instance, the suppression of cold pools and the enhancement of atmospheric instability (Heiblum et al. 2016b).

Clouds that develop above the freezing level are more difficult to model given the complexity of the processes involving ice particles. One aspect of the aerosol effects on clouds is their ability to alter the way in which ice is formed in the mixed phase of convective clouds. Contact freezing is possibly the dominant process by which the first ice is formed (Cooper, 1974; Young, 1974; Lamb et al., 1981; Hobbs and Rangno, 1985). As pointed out by Lohmann and Hoose (2009), anthropogenic aerosol particles can either enhance or hinder cloud glaciation due to primary aerosol emission (increasing INPs concentrations) and aerosol particle coating (decreasing INPs effectiveness), respectively. After the initial ice formation, secondary ice generation can be triggered by the release of ice splinters from freezing droplets (Hallett and Mossop 1974; Huang et al. 2008; Sun et al. 2012; Lawson et al. 2015). Rather big (larger

than 23 μm) cloud and drizzle droplets favor secondary ice generation (Mossop 1978; Saunders and Hosseini 2001; Heymsfield and Willis 2014). Consequently, the smaller droplets found in polluted Amazonian clouds (Andreae et al. 2004; Cecchini et al. 2016; Wendisch et al. 2016) may slow down secondary ice generation.

In order to model aerosol effects on clouds and the thermodynamic feedback processes involved, it is crucial to understand their effects on hydrometeor size distributions. The first step is the study of aerosol impacts on liquid droplet size distributions (DSDs) in the cloud's warm-phase. Operational models that require fast computations usually adopt a Gamma function (Ulbrich, 1983) to parameterize the DSDs:

$$N(D) = N_0 D^{\mu} \exp(-\Lambda D) \quad (1)$$

where N_0 (cm^{-3} μm$^{-1-\mu}$), μ (dimensionless), and Λ (μm^{-1}) are the intercept, shape, and curvature parameters. *N(D)* is the concentration of droplets per cm^{-3} of air and diameter (*D*) bin interval. The units given are the ones to be considered in this study. Even though ~~this~~ the Gamma function is widely adopted in models (Khain et al. 2015), there is almost no study regarding its phase space for checking DSD predictions between parameterization schemes.

The phase space of cloud micro- and macro-physical properties has received recent attention because of the considerable gain of information accessible by relatively simple analysis tools. Heiblum et al. (2016a, b) studied cumulus fields in a two-dimensional (2D) phase space consisting of cloud center of gravity versus water mass. The authors were able to evaluate several processes in this sub-space, including the aerosol effect. McFarquhar et al. (2015) studied the Gamma phase space for improving ice particle size distribution (PSD) fitting and parameterization. They showed that the inherent uncertainty of Gamma fittings results in multiple solutions for a single ice PSD, corresponding to ellipsoids rather than points in the phase space. However, there is no study regarding the representation of warm-phase cloud DSDs in the Gamma phase space and its evolution.

For the representation of hydrometeor size distributions in two-moment bulk schemes, one of the three Gamma parameters is either fixed or diagnosed based on thermodynamic or DSD properties (Thompson et al. 2004; Milbrandt and Yau 2005; Formenton et al. 2013a, 2013b). This process may produce artificial trajectories in the phase space ~~when comparing Gamma fittings to observations~~by limiting the parameter variability. This study analyzes cloud DSD data collected during the ACRIDICON-CHUVA campaign

(Wendisch et al. 2016) in the Gamma phase space. ACRIDICON is the acronym for "Aerosol, Cloud, Precipitation, and Radiation Interactions and Dynamics of Convective Cloud Systems", while CHUVA stands for "Cloud Processes of the Main Precipitating Systems in Brazil: A Contribution to Cloud Resolving Modeling and to the GPM (Global Precipitation Measurement)". The Gamma phase space and its potential use for understanding cloud processes is introduced and explored. A specific focus is on the aerosol effect on the trajectories in the warm-layer phase space and potential consequences for the mixed-phase formation.

Section 2 describes the instrumentation and methodology. The results are presented in Section 3, followed by concluding remarks in Section 4.

2 Methodology

2.1 Flight characterization

During September-October 2014, the German HALO (High Altitude and Long Range Research Aircraft) performed a total of 96 h of research flights over the Amazon. The 14 flights were part of the ACRIDICON-CHUVA campaign (Machado et al. 2014; Wendisch et al. 2016) that took place in cooperation with the second intensive operation period (IOP2) of the GoAmazon2014/5 experiment (Martin et al. 2016). Here we focus on cloud profiling sections during six flights that occurred in different regions in the Amazon (Figure 1). The research flights of ACRIDION-CHUVA were named chronologically from AC07 to AC20; the six flights~~ missions focusing on the profiling of cloud microphysical properties~~ selected (AC07, AC09, AC12, AC13, AC18 and AC19) accumulated 16.8 h of data (in or out of clouds), of which 50 min were inside the lower 6 km of the clouds. We concentrate primarily on the~~se flights~~ first 6 km for the DSD analysis in order to capture both warm-phase characteristics and early mixed-layer formation. There were other flights with cloud penetrations, but they are not considered in this study because of higher aerosol variability below clouds. The flights chosen for analysis presented relatively low aerosol variability, meaning that the clouds probed in the same flight were likely subject to similar aerosol conditions. The time frame of the campaign corresponds to the local dry-to-wet season transition, when biomass burning is active in the southern Amazon (Artaxo et al. 2002, Andreae et al. 2015). For

clarity, the flights of interest are renamed in this study according to the region probed. Flight AC19 will be referred as M1 (Maritime 1), flights AC09 and AC18 as RA1 and RA2 (Remote Amazon 1 and Remote Amazon 2, respectively), and flights AC07, AC12, and AC13 as AD1, AD2, and AD3 (Arc of Deforestation 1, Arc of Deforestation 2, and Arc of Deforestation 3, respectively). Those definitions are listed in Table 1.

The flight paths followed a regular three-stage pattern: (i) Sampling of the air below clouds for aerosol characterization, (ii) Measurements of DSDs at cloud base, and (iii) Sampling of growing convective cloud tops (Braga et al., 201~~6~~7; Wendisch et al., 2016). The latter step was deployed as follows. After the cloud base penetration, the aircraft performed several penetrations in vertical steps of several hundred meters. In each step, the aircraft penetrated the cloud tops available, thus avoiding precipitation from above. In this way, different clouds can be penetrated in the same altitude level and the vertical steps followed the growing cumuli field overall. Surface and thermodynamic conditions were different for the various flights (see Figures 1 and 3) with high contrasts in the north-south direction. Logging, agriculture, and livestock activities management involve burning extended vegetated areas in the region, which emits large quantities of particles that serve as CCN in the atmosphere (Artaxo et al. 2002; Roberts et al. 2003). Because of this, this region is known as the "Arc of Deforestation," and its thermodynamic properties tend toward pasture-like characteristics. The energy partitioning over pasture-like areas is different compared to regions over the rainforest (Fisch et al. 2004), favoring sensible heat flux and higher cloud base heights (see Table 1). Contrasting with the Arc of Deforestation, the region named Remote Amazon in this study has much lower background aerosol concentrations, producing cleaner clouds. Clouds over the Atlantic Ocean developed under cleaner conditions as compared to the continental counterparts, and also had lower cloud bases (Table 1).

The cloud profiling missions were mostly characterized by cumulus fields, with some developed convection in two flights over the Arc of Deforestation (Figure 2d, f). For flight ~~AC07~~ AD1 some precipitation-sized droplets were observed (not shown); the clouds sampled during ~~AC12~~ AD2 and ~~AC13~~ AD3 presented almost no droplets having $D > 100$ µm. The precipitation during ~~AC07~~ AD1 might be explained by the lower aerosol particle number concentrations compared to flights ~~AC12~~ AD2 and ~~AC13~~AD3, later start time of the profile, and the presence of deep convection nearby (Table 1 and Figure 2).

2.2 Data handling and filtering

The results to be presented here are based on five sensors carried by HALO. A comprehensive description of the airborne instrumentation introduced below can be found in Wendisch et al. (2013). Aerosol particle number concentrations (N_{CN}) were measured by a butanol-based Condensation Particle Counter (CPC). The flow rate was set to 0.6 L min^{-1}, with a nominal cut-off particle size of 10 nm. N_{CCN} at a given supersaturation (S, averaging 0.48% ± 0.033% for the data used here, with 10% error) was measured by a Cloud Condensation Nuclei Counter (CCN-200, Roberts and Nenes 2005). This instrument contains two columns and was connected to two different inlet systems for aerosol sampling: the HALO Aerosol Sub-micrometer Inlet (HASI) for the aerosol particles and the Counter-flow Virtual Impactor (CVI) inlet to sample cloud droplets, evaporate the cloud water, and analyze the residual particles. The aerosol measurements reported in this study refer to the HASI inlet.

Cloud DSDs were measured by a Cloud Droplet Probe (CDP, Lance et al. 2010; Molleker et al. 2014) that is part of the Cloud Combination Probe (CCP). The CCP also contained a grayscale Cloud Imaging Probe (CIPgs, Korolev 2007), but we focus on CDP measurements where D < 50 µm. The intent is to focus on cloud droplet growth processes and bringing the analysis closer to modeling scenarios. Additionally, the percentage of data with significant liquid water content (LWC) for D > 50 µm is relatively small. The number of data with $LWC_{D>50}$ > 0.1 g m^{-3} is only 8% of the number of DSDs with $LWC_{D<50}$ > 0.1 g m $^{-3}$. The CDP counted and sized the droplets based on their forward scattering characteristics, sorting them into 15 droplet size bins between 3 µm and 50 µm. The sample volume had an optical cross-section of 0.278 mm^2 (±15%). Uncertainties in the cross-section area, the sampling volume, and counting statistics were the major sources of uncertainty for the DSD measurements (Weigel et al., 2016). According to Molleker et al. (2014), the CDP uncertainty is about 10%. Additionally, Braga et al. (2017) performed an inter-comparison between HALO probes, as well as hot-wire measurements, and concluded that they agree well within instrumental uncertainties. We excluded all cloud DSDs with droplet number concentrations (N_d) less than 1 cm^{-3} from further analysis.

The DSDs measured by the CDP were fitted to Gamma distributions (Eq. 1) by matching the zeroth, second and third moments. These moments were chosen in order to favor the study of the DSD properties of interest to this study (i.e., droplet number concentration, liquid water content, and effective diameter),

but they also coincided with the properties usually predicted by bulk microphysics models (zeroth and third moments in two-moment schemes). The complete Gamma function is used to be consistent with modeling scenarios, ~~The~~ where the Gamma parameters are calculated by:

$$\mu = \frac{6G-3+\sqrt{1+8G}}{2(1-G)} \quad (2)$$

$$\Lambda = \frac{(\mu+3)M_2}{M_3} \quad (3)$$

$$N_0 = \frac{\Lambda^{\mu+1}M_0}{\Gamma(\mu+1)} \quad (4)$$

where M_p is the *p-th* moment of the DSD. The symbol G is a non-dimensional ratio, given as follows:

$$G = \frac{M_2^3}{M_3^2 M_0} \quad (5)$$

The three parameters N_0, μ, and Λ define the Gamma distribution in Eq. (1); they are used to construct the phase space described in the next section. The DSD bulk properties, such as droplet number concentration (N_d), liquid water content (LWC), effective droplet diameter (D_{eff}), and relative dispersion (ε), can be derived from the Gamma parameters N_0, μ, and Λ by taking into account the complete Gamma function integral properties~~:~~. In the units considered here, the equations are given by:

$$N_d = \int_0^\infty N(D)dD = N_0 \frac{\Gamma(\mu+1)}{\Lambda^{\mu+1}} \quad (6)$$

$$LWC = 10^{-9}\frac{\pi}{6}\rho_w \int_0^\infty N(D)D^3 dD = 10^{-9}\frac{\pi}{6}\rho_w N_0 \frac{\Gamma(\mu+4)}{\Lambda^{\mu+4}} \quad (7)$$

$$D_{eff} = \frac{\int_0^\infty N(D)D^3 dD}{\int_0^\infty N(D)D^2 dD} = \frac{\mu+3}{\Lambda} \quad (8)$$

$$\varepsilon = \frac{\sigma}{D_g} = \frac{1}{\sqrt{\mu+1}} \quad (9)$$

where ρ_w = 1000 g m^{-3} represents the density of liquid water and σ and D_g are the DSD standard deviation and mean geometric diameter, respectively. N_d, LWC and D_{eff} are given in cm^{-3}, g m^{-3} and µm, respectively. Given the choice of the conserved moments, they exactly match the respective characteristics of the observed DSDs. The parameter ε is described in detail in Tas et al. (2015). The relative dispersion of the Gamma DSD may differ from the observations, given the differences between the parameterized and observed DSDs. However, ~~O~~our measurements show that the Gamma and observed ε are closely related

by $\varepsilon_{Gamma} = 0.95\varepsilon_{Observed}$ (R^2 = 0.93), showing that the Gamma DSDs are slightly narrower on average. We focus on ε as obtained by the Gamma parameters and do not use subscripts.

Cloud hydrometeor sphericity was analyzed by the NIXE-CAPS probe (New Ice eXpEriment – Cloud and Aerosol Particle Spectrometer, Luebke et al., 2016, Costa et al., 2017). NIXE-CAPS also contains two instruments, a CIPgs as the CCP and the CAS-Depol for particle measurements in the size range 0.6 to 50 µm. The sizing principle of CAS-Depol is similar to the CDP, the difference is the particle probing: while CAS-Depol has an inlet tube (optimized with respect to shattering), CDP is equipped with an open path inlet. In addition to the sizing, CAS-Depol is equipped with a detector to discriminate between spherical and aspherical particles by measuring the change of the polarized components of the incident light. Spherical particles do not strongly alter the polarization state, in contrast to non-spherical ice crystals. The cloud particle phase of the whole cloud particle size spectrum was analyzed from the combination of phase determination in the size ranges < 50 µm (from the CAS-Depol polarization signal) and > 50 µm (from visual inspection of the CIPgs images) (for details, see Costa et al., 2017). Here, the phase states are defined as follows: "Sph (liquid)" stands for many only spherical (D < 50 µm) and predominantly spherical (D > 50 µm) hydrometeors, "Asph small (mixed phase)" for many predominantly spherical (D < 50 µm) and only aspherical (D > 50 µm), "Asph large (ice)" for only very few aspherical (D < 50 µm) and only aspherical (D > 50 µm). The NIXE-CAPS classification is a separate analysis and will not be considered as a filter to apply the Gamma fits to the CDP measurements. The CDP data fits are primarily focused on the warm phase and the transition to the mixed layer, where liquid droplets predominate.

Meteorological conditions, including three-dimensional (3D) winds, were obtained by the Basic HALO Measurement and Sensor System (BAHAMAS) located at the nose of the aircraft (Wendisch et al., 2016). The wind components were calibrated according to Mallaun et al. (2015), with an uncertainty of 0.2 m s^{-1} and 0.3 m s^{-1} for the horizontal and vertical directions, respectively. All probes were synchronized with BAHAMAS and operated at a frequency of 1 Hz. All HALO instruments are listed in Wendisch et al. (2016).

2.3 Introducing the Gamma phase space

The Gamma fit parameters can be plotted in a 3D subspace where each parameter (N_0, μ, and Λ) represents one dimension. Each point in this 3D Gamma phase space is defined by one (N_0, μ, and Λ) triplet and thus represents one fitted DSD. This space includes all possible combinations of Gamma parameters of the theoretical variability of the DSDs.

The 3D Gamma phase space is illustrated in Figure 3. There are two points in this figure defined by two location vectors P_1 and P_2, each one representing a fit to a specific DSD (see the insert in the left side of Figure 3) at different times (t_1 and t_2 for $t_2 > t_1$). If we consider that $\overrightarrow{P_1}$ and $\overrightarrow{P_2}$ represent the same population of droplets evolving in time (i.e., a Lagrangian case), we can link the two points by a displacement vector $\vec{P} = \overrightarrow{P_2} - \overrightarrow{P_1}$, which can be associated to a pseudo-force $\vec{F}$ (blue arrow in Figure 3). We use the term pseudo-force in order to illustrate that the growth processes produce displacements in the phase space. Alternatively, displacements in the phase space can also be understood as phase-state transitions, in which case each phase-state is related to a DSD. The pseudo-force $\vec{F}$ can be decomposed into two components, one related to condensational growth and the other to the collision-coalescence (collection) process. The respective pseudo-forces are illustrated as $\overrightarrow{F_{cd}}$ and $\overrightarrow{F_{cl}}$ in Figure 3, respectively. This approach can be applied to multiple points, defining a trajectory through the phase space (gray dotted line). The change of the DSD results in modified Gamma parameters, which determine the trajectory through the Gamma phase space. The direction and speed of the displacements forming the trajectory are determined by the direction and intensity of the underlying physical processes that modify the DSD (condensation and collection). These pseudo-forces are defined by properties such as the initial DSD, CCN, updraft speed, and supersaturation. Of course, this generalization considers only condensation and collision-coalescence. The pseudo-forces can be represented with more sophistication in models, including the several processes involved in DSD changes, such as evaporation, turbulence, melting from the layer above, breakup, sedimentation, etc. Therefore, these two processes can be replaced by a number of pseudo-forces as function of the level of sophistication of the model. We should remember that this approach does not consider contributions from other levels because advection is not directly addressed. To

describe the whole process of DSD evolution during the entire cloud life cycle, the contribution from other layers should be considered.

The direction of the $\overrightarrow{F_{cd}}$ pseudo-force in Figure 3 represents the transition of the DSD during the condensation process, which favors high values of μ while slightly increasing Λ. This induces both the narrowing and a slight increase in the effective droplet diameter (see equations in Section 2.2) of the DSD, which is expected from conventional condensation growth theory. Because of the DSD narrowing, the intercept parameter (N_0) is also reduced. Condensational growth may cause a broadening of the DSD in specific situations such as at the cloud base of polluted systems. However, this is an exception and most of the time condensational growth leads to DSD narrowing. The collision-coalescence pseudo-force acts in a significantly different way in the phase space. From theory and precise numerical simulations that solve the stochastic collection equation, it is known that this process leads to DSD broadening (given the collection of small droplets and breakup of bigger ones) and faster droplet growth in size (compared to condensation). In the Gamma phase space, it should be reflected in lower values of Λ and μ, the former decreasing at a faster pace. The intercept parameter N_0 ~~should~~ can remain relatively constant or increase, ~~given that~~because the effects of increased mean diameter and DSD broadening balance each other. ~~With~~ If N_0 ~~almost~~ remains constant, lower values of Λ and μ result in reduced droplet number concentration, which is consistent with theory (see Figure 7).

To confirm the overall directions of the pseudo-forces and the characteristics of the Gamma phase-space, we performed some calculations with the Lagrangian model described in Feingold et al. (1999) – see their Section 3c and references therein. Basically, the model solves CCN activation, condensation and collision-coalescence growth, and the effects of giant CCN on the DSDs (the latter process was turned off in our runs). The DSDs are sorted into 35 mass-doubling bins from ~3 μm to ~9 mm, so the condensation and collision-coalescence processes are not parameterized as in bulk approaches. The model was initialized with conditions that mimic flight RA1 (Table 1, Figure 4). By performing two runs, one with exclusively condensational growth and the other with both growth processes, it was possible to isolate their effects on the DSDs. In the run with both processes active, by the time the collection was significant the droplets were big enough (D_{eff} > 25 μm) to grow very slowly by condensation.

From the Langrangian model runs it was possible to calculate the direction of the displacements caused by condensation and collision-coalescence growth in spherical coordinates. For this first introduction of the phase-space, we will focus on the elevation angle φ (from the plane N_0 x μ to the Λ axis) and azimuth angle θ (calculated from the N_0 to the μ axes), when N_0, μ, and Λ are in logarithm (base 10) scale (as in Figures 5-8). The angles vary depending on the relative values of N_0, μ, and Λ, but the following numbers are provided as a first look into it. For condensational growth, φ averaged 0.26 ° and θ averaged 179.6 °, while they were -4.23 ° and -13.7 ° for collision-coalescence, respectively. Note that the angles have opposite signs for the two processes and their overall direction is the same as exemplified in Figure 3. The direction of the displacements remains consistent even when other moments are chosen to fit the Gamma DSDs. For more details on the model runs, refer to the supplement material.

Note that, given the relation between the Gamma parameters, the phase-space is non-orthogonal and it is not trivial to represent mathematically the pseudo-forces. The mathematical treatment of such forces is beyond the scope of this paper, which intends to illustrate microphysical processes in the phase-space. But this aspect should be considered in potential future implementations of this methodology in practical applications.

In Section 3.2, we show Gamma parameters fitted to real DSD observations. ~~It~~ As it is not feasible to follow fixed populations of droplets in a Lagrangian way with an aircraft~~. Therefore~~, the evolutions we analyze in the Gamma space are not strictly over time. As a compromise, we use the altitude above cloud base (H) of the measurements instead of time evolution, given the conditions of the measurements and our data handling. The cloud profiling missions were planned to capture growing convective elements before reaching their mature state, which is the reason why they usually started at around 12:00 local time. Additionally, we only consider DSD measurements where updraft speed $w > 0$ in order to focus on the ascending part of the growing clouds.

Another point to take into consideration are the ellipsoids discussed in McFarquhar et al. (2015). Basically, by considering the instrument and Gamma fitting uncertainties, it is possible to define volumes (with ellipsoid shapes) rather than individual points in the Gamma phase space. Inside each ellipsoid, all DSDs are equally realizable and therefore the movements within it have no particular physical meaning and are statistically the same. In this study, however, we estimate that the results evolve beyond individual

Formatado: Fonte: Itálico
Formatado: Fonte: Itálico
Formatado: Fonte: Itálico
Formatado: Fonte: Itálico
Formatado: Fonte: Itálico
Formatado: Fonte: Itálico
Formatado: Fonte: Itálico
Formatado: Fonte: Itálico
Formatado: Fonte: Itálico
Formatado: Fonte: Itálico
Formatado: Fonte: Itálico
Formatado: Fonte: Itálico
Formatado: Não Realce

ellipsoids and the patterns are associated to physical processes. The results shown in the next sections will not consider the ellipsoid approach, but the points shown can be considered to be the central points of such volumes.

3 Results

3.1 Aerosol and thermodynamic conditions in different Amazonian regions

The HALO flights are classified according to the region they covered and the respective aerosol and CCN number concentrations (Table 1). Note the close link between region of the measurements and the aerosol concentrations. From the most pristine clouds at the coast to the most polluted cases in the Arc of Deforestation, there is a ten-fold increase in N_{CN}. Remote regions in the Amazon have aerosol particle concentrations slightly higher than over the coast, which is one of the reasons for the term "Green Ocean" used for the unpolluted Amazon regions (Williams et al., 2002). Flights ~~AC07~~AD1, ~~AC12~~ AD2 and ~~AC13~~ AD3 present flight ~~patterns~~ paths progressively shifted to the south, which are accompanied by increasing values of N_{CN} and N_{CCN}. The farther away the flights take place from the forest, and consequently closer to developed regions, the higher are the pollution levels.

Cloud profiles started at the end of the morning or beginning of the afternoon. The flights were specifically planned for this time period because the convective systems are usually in their developing stages at this time. The freezing level varied between 4500 and 5000 m, while cloud base altitudes were more variable (500 to 2000 m), which resulted from the regional meteorological conditions (Figure 4), and which affects the characteristics of the cloud layers. Clouds in the Arc of Deforestation grow from drier air, given the diminished evapotranspiration rate, and form higher in the atmosphere. As a result, there are thinner warm layers in the polluted clouds, which reduces the time available for droplets to grow by collision-coalescence. Flight ~~AC18~~ RA2 was characterized by a just slightly higher depth of the warm layer compared to the polluted clouds, partly due to the lower altitude of the freezing level. Nevertheless, cleaner clouds can present warm layers 1000 m thicker than clouds affected by pollution.

The vertical profile of the relative humidity (RH) should also be taken into account when comparing clouds formed over different regions. Figure 4b shows that all clouds measured formed in a surrounding~~s~~

environment with RH between 60 % and 90 % for their lower 2500 m layer, being higher for forested areas compared to the Arc of Deforestation. For 2500 m and above, there was a significant drying of the atmosphere for flights ~~AC19~~M1, ~~AC18~~ RA2 and ~~AC12~~AD2. It is not clear if the other flights presented similar behavior given the relatively low data coverage for this layer. Regardless, surrounding dry air can significantly enhance the entrainment mixing process (Korolev et al., 2016). As pointed out by Freud et al. (2008), the mixing in Amazonian convective clouds (and also in other regions – Freud et al., 2011) tends toward the extreme inhomogeneous mixing case, where the effective droplet diameter D_{eff} presents almost no sensitivity to the entrainment. Our result largely corroborates this finding (see Figure 11). It should be pointed out, however, that the recent studies by Korolev et al. (2016), Pinsky et al. (2016a), and Pinsky et al. (2016b) show that homogeneous and inhomogeneous mixing can be indistinguishable depending on meteorological conditions and DSD characteristics when considering the time-dependent characteristics of the entrainment process. Mixing processes may have an impact on the shape of the DSDs measured, thus affecting displacements in the Gamma phase space. The specific type of mixing responsible for it, however, is beyond the scope of this work.

3.2 Observed trajectories in the Gamma phase space

In this study, we use the Gamma phase space as a means to study DSD variability. As described in Section 2.3, this space is obtained when the DSD measurements are fitted to Eq. 1, and N_0, μ, and Λ are used as the dimensions of the 3D subspace. In this space, each point represents one DSD. As the different DSDs were obtained close to the cloud top at the time of the cloud development, the ensemble of positions in the Gamma phase space can be hypothesized as the evolution of the DSDs of a typical cloud through stages of its life cycle. The sequential connection of points (here we use cubic spline fits for illustrating purposes) can be considered as trajectories describing multiple processes responsible for the DSD variability observed. The advantage of using this space is that this variability can be readily observed and compared between different cloud life cycles with different properties. Given the relations between Gamma parameters and DSD properties (Section 2.2), the variability of all cloud microphysical properties can also be inferred from the points in the trajectories. We limited the analysis regarding cloud DSDs and

the Gamma phase space to the regions in which $w > 0$ in order to capture the developing parts of the growing convective elements.

Figures 5 to 7 show the Gamma phase space for all profiles considered in this study, grouped by region. The coloring represents the altitude above cloud base (H), with the 1 Hz measurements shown as small markers. Bigger markers represent averages at every 200-m vertical interval with available information. Curves (or trajectories) represent cubic spline fits to the averaged points. At first glance, it is possible to see ~~significant overall~~stronger differences between the trajectories in the different regions, while internal variations are much weaker. Aerosol concentrations seem to be a key factor controlling warm-phase properties in the Amazon, so the internal similarities can be attributed to similar pollution conditions. On the other hand, differences between the regions stem from the different weights of growth processes. Pristine clouds, like the ones found over the remote Amazon and the coast of the Atlantic Ocean, are characterized by faster droplet growth with altitude associated with enhanced collisional growth. In the Gamma space, this is seen as diagonally-tilted trajectories in Figures 5 and 6, contrasting with the more vertical trajectories found in polluted clouds (Figure 7).

The differences of the DSD variability in each region highlight the relation of growth processes and trajectories in the Gamma phase space. From the theory described in Section 2.3, it is expected that collisional growth results in diagonal trajectories where the droplets get progressively bigger with DSD broadening. Pristine clouds over the coast and remote Amazon show such tilting (Figures 5-6), indicating that this process is effective in these systems. The more vertically-oriented trajectories of polluted clouds (Figure 7) show that there is a different balance between condensational and collisional growth. In terms of the Gamma phase space characteristics, this can be understood as weaker $\overrightarrow{F_{cl}}$ as a result of smaller droplets and narrower DSDs. This highlights that the interaction between aerosols and collisional growth occurs mainly through changes in the initial DSD (i.e., P_1 in Figure 3). For each point in the Gamma phase space the collisional pseudo-forces have different intensities and directions, suggesting that a vector field can be constructed. This could only be achieved by idealized model experiments, however, where the updraft speeds can also be prescribed.

Condensational growth can also be illustrated by some points in Figures 6 and 7. Under polluted conditions, this type of growth is expected to be dominant close to cloud base where the droplets are too small

to trigger collision-coalescence. In Figure 7, this is seen in the first 2 or 3 points in the trajectories (dark blue colors), where the points evolve to higher μ values with altitude. This results in DSD narrowing and almost opposite displacement in the Gamma space compared to collisional growth. This trend is shifted when the altitude is reached where collection processes start to become relevant. Another example of condensational growth can be seen in Figure 6 at 3000 m. At this point, which is close to the freezing level, there is a sudden increase in the updrafts (see Tables 2 and 3) and consequently increased condensation rates. The rapid increase in condensational growth, with no significant changes in collision-coalescence, tilts the trajectories to a direction similar to that observed close to cloud base in polluted systems. The displacement is closer to the horizontal direction (i.e., the plane N_0 x μ), because droplets are growing concomitantly by collision-coalescence in the cleaner clouds.

The magnitude of the condensational pseudo-force ($\overrightarrow{F_{cd}}$ in Figure 3) also depends on the initial DSD characteristics (P_1). Condensational growth rates are inversely proportional to droplet size, meaning that they get weaker higher in the cloud. The different dependences of $\overrightarrow{F_{cd}}$ and $\overrightarrow{F_{cl}}$ on P_1 and their balance throughout the warm-phase life cycle ultimately define the cloud trajectory in the phase space. If they can be mapped with sufficient resolution, covering different updraft and supersaturation conditions, trajectories may be forecast from a single DSD at cloud base and the evolving thermodynamic conditions. Aerosols are a key aspect in this regard because they significantly change the cloud-base-DSD in the Gamma space (Figures 5-7) and also affect cloud thermodynamics, impacting condensation rates and consequently latent heat release. Note that clouds subject to similar aerosol conditions have similarities in their trajectories represented by small variability along the trajectories of the respective flights (Figures 6-7).

The $\overrightarrow{F_{cd}}$ and $\overrightarrow{F_{cl}}$ tabulation over the Gamma space can potentially be achieved with the help of Lagrangian large-eddy-simulation bin-microphysics models that precisely solve the condensation and collection equations for varying input DSDs and updraft conditions. Initial DSDs can be obtained from observations and analytical considerations. For instance, Pinsky et al. (2012) show an analytical way to obtain the maximum supersaturation (which is usually a few meters above cloud base) and the relative droplet concentration. If D_{eff} behaves adiabatically (Freud et al., 2008; Freud et al., 2011) and is linearly correlated to the mean volumetric diameter (Freud and Rosenfeld, 2012), it is possible to estimate the initial DSD based on Gamma-DSD equations and adiabatic theory given that the aerosol population is known. The

advantage of such approach is that all DSD characteristics, most notably its shape, would be realistically represented and there would be no need for fixing or diagnosing (Thompson et al. 2004; Milbrandt and Yau 2005; Formenton et al. 2013a, 2013b) Gamma parameters for various hydrometeor types – which works for specific applications but may be lacking the physical representation of the processes. This study focuses on introducing the Gamma phase space and its characteristics, and further work is needed if new parameterizations are to be developed.

3.3 Contrasts between clean and polluted trajectories

In this section, we focus on flights ~~AC09~~ RA1 and ~~AC12~~ AD2 in order to study the differences between natural and human-affected clouds in the Gamma space. Figure 8 shows the trajectories of the clouds measured during these flights, where the points related to the averaged DSDs are numbered and the corresponding properties are shown in Tables 2-3. The numbers start at 1 close to cloud base and grow with altitude ("p" stands for "polluted", while "c" is for "clean"). Also presented in Tables 2 and 3 are the adiabatic fractions which correspond to the ratio between the observed and adiabatic LWC. Some observed DSDs and their corresponding Gamma DSDs are shown in Figure 9, highlighting different growth processes.

It is clear from Figure 8 that clean and polluted clouds cover different regions of the Gamma phase space. Nevertheless, it is possible to see that the trajectories can evolve almost in parallel depending on the dominant growth process. Polluted clouds have wider DSDs at cloud base because of the tail to lower diameters (Figure 9), which brings down the value of μ (see Eq. 9). Given the lower droplet size (Table 3), condensation is efficient and the trajectories evolve in the overall direction of $\overrightarrow{F_{cd}}$ illustrated in Figure 3. From point 1p to 2p, N_d and LWC are approximately doubled. Condensational growth seems to be the dominant growth process in the polluted clouds up to the point 3p, corresponding to a cloud depth of 600 m. A similar layer does not exist in cleaner clouds, where there are enough big droplets to readily activate the collision-coalescence growth. Collisional growth dominates the DSD shape evolution between points 1c and 6c for flight ~~AC09~~ RA1 and between 4p and 7p for ~~AC12~~AD2. Note that the trajectories are almost parallel in this region. Condensation is still active in this period given the increasing LWC, but collision-

coalescence have a comparatively bigger impact on the overall DSD shape. Both sections of the trajectories represent 1400-m thick layers, but droplet growth and DSD broadening is more efficient in the cleaner clouds (Figure 9). This explains the pronounced tilting of its trajectory, consistent with a stronger $\overrightarrow{F_{cl}}$ pseudo-force.

Eventually, the trajectories reach a point close to the 0 °C isotherm where the updrafts are enhanced given the continued latent heat release. This *w*-enhanced layer can be several hundred meters thick and culminates in narrower DSDs. This is exemplified between points 7c and 9c and between 8p and 10p. Although droplets are still growing by collision-coalescence, the enhanced updrafts increase condensational growth sufficiently to produce observable effects on the DSDs. Both trajectories evolve in the condensational growth direction, but with slightly different tilting. The tilting is less pronounced in the cleaner clouds given the stronger $\overrightarrow{F_{cl}}$ component. The way in which the DSDs evolve in this region is important for the mixed-phase initiation, given that both primary and secondary ice generation depend on the characteristics of the liquid droplets. The different properties of the polluted and clean DSDs (see Tables 2 and 3, Figures 8 and 9) indicate that ice formation may follow distinct pathways.

Previous studies suggest that droplets bigger than 23 μm at concentrations higher than 1 cm^{-3} favor secondary ice generation, which was identified as the main mechanism for cloud glaciation (Mossop 1978; Saunders and Hosseini 2001; Heymsfield and Willis 2014; Lawson et al. 2015). In order to visualize these conditions in the Gamma phase space, it is interesting to consider constant N_d surfaces. These surfaces are defined when N_d is fixed in Eq. 6, resulting in a relation of the form $\Lambda = f(N_0, \mu)$ when inverted. Examples are shown in Figure 10, where N_d = {10, 100, 1000} cm^{-3} (axes are rotated for clarity). The surfaces are evidently parallel and are stacked in relatively close proximity (at the scale used here). The trajectories evolve through the surfaces depending on their N_d, where polluted clouds tend toward higher droplet concentration (i.e., closer to the red surface). These surfaces can be used to delimit specific regions of interest. Additionally, further DSD properties can be analyzed along these surfaces. Figure 10 highlights the region of 23 μm < D_{eff} < 50 μm with black lines along the surface of N_d = 10 cm^{-3}. Regarding cloud DSDs (drizzle droplets are not analyzed here, although they also contribute to ice formation), the region delimited by the black lines for the different surfaces of constant N_d can be interpreted as the most favorable for secondary ice generation, thus indicating a quick glaciation process. Note that the trajectory

of the cleaner clouds enters this region while in the *w*-enhanced layer mentioned previously, which corresponds to the transition to temperatures below 0 °C. Polluted clouds are able to produce high droplet number concentrations, but their smaller droplet size means that they are out of the delimited region. More details about the transition to the mixed phase are given in the next section.

The observation of constant N_d surfaces poses an interesting question for parameterizations. In existing two moment schemes, both N_d and LWC are predicted. For each pair of such properties, it is possible to define two surfaces (with constant N_d and LWC, respectively) based on Eqs. 6 and 7. These surfaces intersect, defining a curve where both properties are conserved. In this curve, the mean volumetric diameter (proportional to the ratio between LWC and N_d) is also constant. Based on the limited information provided by the model (only two moments for three Gamma parameters), this curve represents the infinite DSD solutions for the undetermined equation system. A good parameterization scheme should be able to choose one of the DSDs that best fits observations. Given the undetermined equation system, other considerations have to be made.

One parameter that varies along the infinite DSD solution curve is the relative dispersion ε. If ε ~~is calculated from theoretical considerations or provided by observations~~can be constrained in the model, it should be possible to obtain the full Gamma DSD – which is the point in the intersection curve that presents the given ε. The advantage of relying on ε is that it has low variability between clean and polluted clouds and its average is almost constant with altitude. Tas et al. (2015) studied the relative dispersion parameter in detail, noting that averaged values for ε were independent of N_d, LWC, or height but its variability is significantly lower for the most adiabatic portions of the cloud (notably its updraft core). For precise parameterizations, ε variability should be taken into account at regions with relatively low N_d and LWC, but averaged values may be considered for the updraft cores. Our observations show that ε is slightly higher in polluted Amazonian clouds compared to the ones measured over remote regions mainly because of their reduced droplet size (Tables 2 and 3). This can be considered to produce slight corrections to ε based on CCN number concentrations.

3.4 Observations of the mixed phase formation

The Gamma phase space provides an insightful way to study the formation of the mixed phase by providing the history of the warm phase development as a trajectory. Liquid cloud droplet properties are important for the glaciation process because they determine the probability of contacting ice nucle~~i~~ating particles (INPs) and the conditions for secondary generation. As shown in the previous sections, different aerosol and thermodynamic conditions alter warm phase characteristics and can thus impact the early formation of ice in the clouds.

Figure 11 shows vertical profiles of N_d, LWC, D_{eff}, and ε for clouds subject to background and polluted conditions (flights ~~AC09~~ RA1 and ~~AC12~~AD2, respectively). It shows the different microphysical properties (1 Hz) of the clouds associated with the trajectories presented in Figures 8 to 10 ($w > 0$). It shows that droplet concentrations are much higher in polluted clouds, which are not depleted with altitude as much as cleaner clouds (Figure 11a, b). The lower effective diameter for clouds over the Arc of Deforestation may contribute to enhanced evaporation, leading to lower adiabatic fractions. As commented in the previous section, ε shows small variations between the flights and do not change much with altitude. The properties of the DSDs around the 0 °C level in Figure 11 are a significant feature regarding the mixed phase formation. Note that cleaner clouds have a sudden change in behavior right above the freezing level. At this point, there is a fast decrease in LWC, with higher variability in both D_{eff} and ε. This suggests that ice processes have been triggered, disrupting the smooth evolution observed in the warm phase. In polluted clouds, this transition takes place at considerably different DSD properties. Averaged N_d reaches values above 1000 cm^{-3} (compared to 50 cm^{-3} in cleaner clouds) with very strong updrafts, bringing LWC closer to adiabaticity. However, no significant variability was observed for D_{eff}, suggesting that most of the water is still in condensed state.

In order to further detail the characteristics of the hydrometeors in the transition from warm to mixed phase, we analyzed the sphericity criteria obtained by the NIXE-CAPS probe (Costa et al., 2017). The methodology developed by Costa et al. (2017) indicates whether each individual 1 Hz measurement contained some aspherical hydrometeors or not. This criterion can be used to indicate whether the hydrometeors are liquid (spherical), mixed (spherical and aspherical), or frozen (aspherical). By combining all

measurements for clouds over the remote Amazon (~~AC09~~ RA1 and ~~AC18~~RA2) and the Arc of Deforestation (~~AC07~~AD1, ~~AC12~~ AD2 and ~~AC13~~AD3), we obtained the results shown in Figure 12.

The classifications shown in Figure 12 separate the volumes probed as containing only spherical hydrometeors ("Sph (liquid)") or if there are also aspherical particles too. In that case, the data are further divided into containing both small (D < 50 μm) spherical and large aspherical (D > 50 μm) – "Asph small (mixed phase)" – or if there are only large (D > 50 μm) aspherical particles – "Asph large (ice)". It is possible to observe that close to cloud base most of the hydrometeors were detected as spherical for both regions, which is expected given that it is the warmest layer of the cloud. However, higher in the clouds the distribution of the classifications become different. The amount of measurements with aspherical particles increases relatively fast for the cleaner clouds, being higher than 90% at the layer around 0 °C. For polluted clouds, on the other hand, almost half of the measurements contained exclusively spherical hydrometeors at this level. Exclusively spherical hydrometeors persisted with a frequency of ~20 % down to temperatures of -15 °C. This is in line with previous studies that found supercooled droplets high into continental convective systems (Rosenfeld and Woodley, 2000; Rosenfeld et al., 2008). Our results show that the persistence of supercooled droplets in Amazonian clouds is more likely under polluted conditions. The characteristics of the cloud warm layer determine the properties of the liquid DSDs close to the 0 °C level and should have a determining role in the glaciation initiation. Our measurements show that clean clouds can produce droplets roughly twice the size of the ones found in polluted systems at this layer, at 95 % lower droplet concentrations (Tables 2 and 3). Bigger droplets are not only more likely to interact with INPs and glaciate by immersion or contact freezing, but may also trigger a cascading effect through secondary ice generation (Heymsfield and Willis, 2014; Lawson et al., 2015). This process is able to quickly glaciate the cloud, which fits the results shown in Figure 12. Beyond the DSD bulk properties, the Gamma phase space can also provide more information regarding the kind of DSD that enables or inhibits the glaciation process. In the present study, we have only a few examples to compare warm- and mixed-phase characteristics, but it is clear that it is possible to correlate some regions of the phase space with the characteristics of the ice initiation. Detailed model experiments would greatly enrich this discussion by providing control over the liquid DSD properties and the resulting formation of the mixed layer.

More specifically, it would be invaluable to study the impacts of the properties of DSDs at cloud base and at the 0 °C isotherm on the primary and secondary ice production.

4 Concluding remarks

Despite being widely adopted in many modeling and remote sensing applications, there is almost no study analyzing the evolution of cloud droplet size distributions in Gamma phase space. Here, we introduce this visualization, defined by the intercept, shape, and curvature of the Gamma curve, which is parameterized by obtaining the moments of order zero, two, and three. We show that trajectories in the space are related to DSD evolution and are linked to microphysical processes taking place inside the cloud. These processes can be understood as pseudo-forces in the phase space.

Measurements over the Amazon during the ACRIDICON-CHUVA and GoAmazon2014/5 campaigns show that it is possible to relate the direction of the pseudo-forces to different DSD growth processes. Cloud layers with strong updrafts and consequently relatively strong condensational growth showed that this process induces displacements in the direction of high shape and curvature parameters. This tendency is accompanied by DSD narrowing, consistent with condensational growth theory. On the other hand, collision-coalescence, observable in clean clouds over the Amazon, favors displacements in roughly the opposite direction. Observed displacements in the warm phase may be interpreted as a combination of both pseudo-forces.

The Gamma phase space can also be used as a diagnostic tool for cloud evolution. By studying the displacements in the warm phase, it is possible to determine regions that favor, for instance, cloud glaciation. Previous studies have identified cloud conditions that favor rapid secondary ice generation, which can be translated into the phase space. We show that clean clouds over the Amazon evolve into the region that favors secondary ice generation because of the enhanced collisional growth. Droplets in polluted clouds take much longer to grow by warm processes and they cross 0 °C long before reaching the region favorable for glaciation. This leads to the persistence of supercooled droplets higher in the clouds, which interact with other ice processes including sublimation to produce big ice particles through the Wegener-Bergeron-Findeisen mechanism. In this regard, the Gamma phase space approach proves to be an interesting tool to analyze the relation between warm microphysics and the evolution of the mixed phase.

More studies are encouraged in that direction, especially in modeling scenarios given the difficulties in the prediction of mixed phase processes.

We propose that the Gamma space can be used to both evaluate current parameterization and steer the development of new ones. The results presented here show that different types of clouds have different trajectories through the Gamma phase space. The aerosol effect seems to play a major role in the trajectories of the warm layer. The ability of current parameterizations to reproduce such aspects can be tested in the phase space, where artificially produced DSDs would be apparent. For new two-moment parameterizations, the Gamma space can be used to constrain the DSD from the given droplet concentration and liquid water content. For each pair of these properties, the possible DSD solutions lie on a curve in the Gamma space where the main differentiating factor is the distribution relative dispersion. Observations such as the ones shown here and in previous studies can be used to find the appropriate relative dispersion value to find the optimal solution. Additionally, precise bin microphysics simulations can be used in order to produce full condensational and collisional pseudo-force fields in the space. The fields would be dependent on the evolution of properties such as aerosol concentration, updraft speed, and supersaturation conditions. With such a tabulation, bulk microphysical models would only need to predict the initial DSD close to cloud base and the rest would be determined by the pseudo-force fields.

This paper shows just an initial view of potential applications of the Gamma space. Future efforts are encouraged in order to test its efficiency and adequacy. Currently, we are performing bin microphysics simulations in a column model to compare different closures in bulk schemes. Additionally, we are in the process of testing the use of the Gamma space in a nowcasting scenario based on dual-polarization radar retrievals.

Acknowledgements: The ACRIDICON-CHUVA campaign was supported by the Max Planck Society (MPG), the German Science Foundation (DFG Priority Program SPP 1294), the German Aerospace Center (DLR), the FAPESP (Sao Paulo Research Foundation) grants 2009/15235-8 and 2013/05014-0), and a wide range of other institutional partners. It was carried out in collaboration with the USA–Brazilian atmosphere research project GoAmazon2014/5, including numerous institutional partners. We would like to thank the Instituto Nacional de Pesquisas da Amazonia (INPA) for local logistic help prior, during and

after the campaign. Thanks also to the Brazilian Space Agency (AEB: Agencia Espacial Brasileira) responsible for the program of cooperation (CNPq license 00254/2013–9 of the Brazilian National Council for Scientific and Technological Development). The contribution of Dr. Rosenfeld was supported by project BACCHUS European Commission FP7-603445. Micael A. Cecchini was funded by FAPESP/CAPES grants 2014/08615-7 and 2014/21189-7. B. Weinzierl would like to acknowledge funding by the Helmholtz Association (Grant number VH-NG-606, AerCARE) and by the European Research Council under the European Community's Horizon 2020 research and innovation framework program/ERC Grant Agreement 640458 (A-LIFE). The entire ACRIDICON-CHUVA project team is gratefully acknowledged for collaboration and support. We also acknowledge the contributions from the four Anonymous Referees and thanks Graham Feingold for providing the Lagrangian model cited in the text. The observational data used in this study can be found at http://www.halo.dlr.de/halo-db/.

References

Albrecht, B.A.: Aerosols, cloud microphysics, and fractional cloudiness. Science 245, 1227–1230, 1989.

Andreae, M. O., Rosenfeld, D., Artaxo, P., Costa, A. A., Frank, G. P., Longo, K. M., and Silva-Dias, M. A. F.: Smoking Rain Clouds over the Amazon, Science, 303, 1337–1342, 2004.

Andreae, M. O., Acevedo, O. C., Araùjo, A., Artaxo, P., Barbosa, C. G. G., Barbosa, H. M. J., Brito, J., Carbone, S., Chi, X., Cintra, B. B. L., da Silva, N. F., Dias, N. L., Dias-Júnior, C. Q., Ditas, F., Ditz, R., Godoi, A. F. L., Godoi, R. H. M., Heimann, M., Hoffmann, T., Kesselmeier, J., Könemann, T., Krüger, M. L., Lavric, J. V., Manzi, A. O., Lopes, A. P., Martins, D. L., Mikhailov, E. F., Moran-Zuloaga, D., Nelson, B. W., Nölscher, A. C., Santos Nogueira, D., Piedade, M. T. F., Pöhlker, C., Pöschl, U., Quesada, C. A., Rizzo, L. V., Ro, C.-U., Ruckteschler, N., Sá, L. D. A., de Oliveira Sá, M., Sales, C. B., dos Santos, R. M. N., Saturno, J., Schöngart, J., Sörgel, M., de Souza, C. M., de Souza, R. A. F., Su, H., Targhetta, N., Tóta, J., Trebs, I., Trumbore, S., van Eijck, A., Walter, D., Wang, Z., Weber, B., Williams, J., Winderlich, J., Wittmann, F., Wolff, S., and Yáñez-Serrano, A. M.: The Amazon Tall Tower Observatory (ATTO): overview of pilot measurements on ecosystem ecology, meteorology, trace gases, and aerosols, Atmos. Chem. Phys., 15, 10723-10776, doi:10.5194/acp-15-10723-2015, 2015.

Arakawa, A.: The cumulus parameterization problem: Past, present, and future. J. Climate, 17, 2493–2525, 2004.

Artaxo, P., Martins, J. V., Yamasoe, M. A., Procópio, A. S., Pauliquevis, T. M., Andreae, M. O., Guyon, P., Gatti, L. V., and Leal, A. M. C.: Physical and chemical properties of aerosols in the wet and dry seasons in Rondônia, Amazonia, J. Geophys. Res., 107, 8081, doi:10.1029/2001JD000666, 2002.

Braga, R. C., Rosenfeld, D., Weigel, R., Jurkat, T., Andreae, M. O., Wendisch, M., Pöhlker, M. L., Klimach, T., Pöschl, U., Pöhlker, C., Voigt, C., Mahnke, C., Borrmann, S., Albrecht, R. I., Molleker, S., Vila, D. A., Machado, L. A. T., and Artaxo, P.: Comparing parameterized versus measured microphysical properties of tropical convective cloud bases during the ACRIDICON–CHUVA campaign~~Comparing calculated microphysical properties of tropical convective clouds at cloud base with measurements during the ACRIDICON-CHUVA campaign~~, Atmos. Chem. Phys.~~ Discuss.~~, 17, 7365-7386, https://doi.org/10.5194/acp-17-7365-2017, 2017~~doi:10.5194/acp-2016-872, in review, 2016~~.

Cecchini, M. A., Machado, L. A. T., Comstock, J. M., Mei, F., Wang, J., Fan, J., Tomlinson, J. M., Schmid, B., Albrecht, R., Martin, S. T., and Artaxo, P.: Impacts of the Manaus pollution plume on the microphysical properties of Amazonian warm-phase clouds in the wet season, Atmos. Chem. Phys., 16, 7029-7041, doi:10.5194/acp-16-7029-2016, 2016.

Cooper, W.A.: A possible mechanism for contact nucleation. J. Atmos. Sci., 31: 1832-1837, 1974.

Costa, A., Meyer, J., Afchine, A., Luebke, A., Dorsey, J. R., Gallagher, M. W., Ehrlich, A., Wendisch, M., Baumgardner, D., Wex, H., and Krämer, M.: Classification of Arctic, Mid-Latitude and Tropical Clouds in the Mixed-Phase Temperature Regime, to be submitted to ACP, 2017.

Fan, J., Zhang, R., Li, G., Tao, W.-K., and Li, X.: Simulations of cumulus clouds using a spectral bin microphysics in a cloud resolving model. J. Geophys. Res. 112, D04201. http://dx.doi.org/10.1029/2006JD007688, 2007.

Fan, J., Wang, Y., Rosenfeld, D., and Liu, X.: Review of Aerosol-Cloud Interactions: Mechanisms, Significance and Challenges, Journal of the Atmospheric Sciences, ~~in press~~73, 4221-4252, doi:10.1175/JAS-D-16-0037.1, 2016.

Feingold, G., Cotton, W. R., Kreidenweis, S. M., and Davis, J. T.: Impact of giant cloud condensation nuclei on drizzle formation in marine stratocumulus: Implications for cloud radiative properties. J. Atmos. Sci., 56, 4100-4117, 1999.

Fierro, A. O., Simpson, J., LeMone, M. A., Straka, J. M., and Smull, B. F.: On how hot towers fuel the Hadley cell: An observational and modeling study of line-organized convection in the equatorial trough from TOGA COARE. J. Atmos. Sci., 66, 2730–2746, 2009.

Fierro, A. O., Zipser, E. J., LeMone, M. A., Straka, J. M., and Simpson, J. M.: Tropical oceanic hot towers: Need they be undilute to transport energy from the boundary layer to the upper troposphere effectively? An answer based on trajectory analysis of a simulation of a TOGA COARE convective system. J. Atmos. Sci., 69, 195–213, 2012.

Fisch, G., Tota, J., Machado, L. A. T., Dias, M., Lyra, R. F. D., Nobre, C. A., Dolman, A. J., and Gash, J. H. C.: The convective boundary layer over pasture and forest in Amazonia, Theor. Appl. Climatol., 78, 47–59, 2004.

Formenton, M., Phillips, V. T. J., and Lienert, B.: A new snow microphysics parameterization applied to a cloud electrification model: Framework and preliminary results, 93rd AMS Annual Meeting, Austin, Tex., 6–10 Jan, 2013a.

Formenton, M., Panegrossi, G., Casella, D., Dietrich, S., Mugnai, A., Sano, P., Di Paola, F., Betz, H.-D., Price, C., and Yair, Y.: Using a cloud electrification model to study relationships between lightning activity and cloud microphysical structure, Nat. Hazards Earth Syst. Sci., 13, 1085–1104, doi:10.5194/nhess-13-1085-2013, 2013b.

Freud, E., Rosenfeld, D., Andreae, M. O., Costa, A. A., and Artaxo, P.: Robust relations between CCN and the vertical evolution of cloud drop size distribution in deep convective clouds, Atmos. Chem. Phys., 8, 1661–1675, doi:10.5194/acp-8-1661-2008, 2008.

Freud, E., Rosenfeld, D., and Kulkarni, J. R.: Resolving both entrainment-mixing and number of activated CCN in deep convective clouds, Atmos. Chem. Phys., 11, 12887-12900, doi:10.5194/acp-11-12887-2011, 2011.

Freud E., Rosenfeld D.: Linear relation between convective cloud drop number concentration and depth for rain initiation. J. Geophys. Res., 117, D02207, doi:10.1029/2011JD016457, 2012.

Gonçalves, W. A., Machado, L. A. T., and Kirstetter, P.-E.: Influence of biomass aerosol on precipitation over the Central Amazon: an observational study, Atmos. Chem. Phys., 15, 6789-6800, doi:10.5194/acp-15-6789-2015, 2015.

Hallett, J., Mossop, S.C.: Production of secondary ice particles during the riming process. Nature 249, 26–28, 1974.

Heiblum, R. H., Altaratz, O., Koren, I., Feingold, G., Kostinski, A. B., Khain, A. P., Ovchinnikov, M., Fredj, E., Dagan, G., Pinto, L., Yaish, R., and Chen, Q.: Characterization of cumulus cloud fields using trajectories in the center-of-gravity vs. water mass phase space: 1. Cloud tracking and phase space description, J. Geophys. Res., 121, doi:10.1002/2015JD024186, 2016a.

Heiblum, R. H., Altaratz, O., Koren, I., Feingold, G., Kostinski, A. B., Khain, A. P., Ovchinnikov, M., Fredj, E., Dagan, G., Pinto, L., Yaish, R., and Chen, Q.: Characterization of cumulus cloud fields using trajectories in the center of gravity versus water mass phase space: 2. Aerosol effects on warm convective clouds, J. Geophys. Res., 121, 6356–6373, doi:10.1002/2015JD024193, 2016b.

Heymsfield, A., and Willis, P.: Cloud conditions favoring secondary ice particle production in tropical maritime convection. J. Atmos. Sci. 71, 4500–4525, 2014.

Hobbs, P.V., and Rangno, A.L.: Ice particle concentrations in clouds. J. Atmos. Sci., 42: 2523-2449, 1985.

Huang, Y., Blyth, A., Brown, P., Choularton, T., Connolly, P., Gadian, A., Jones, H., Latham, J., Cui, Z., and Carslaw, K.: The development of ice in a cumulus cloud over southwest England. New J. Phys. 10, 105021, 2008.

Khain, A., Rosenfeld, D., and Pokrovsky, A.: Aerosol impact on the dynamics and microphysics of convective clouds, Q. J. R. Meteorol. Soc., 131, 2639–2663, doi:10.1256/qj.04.62, 2005.

Khain, A. P., Beheng, K. D., Heymsfield, A., Korolev, A., Krichak, S. O., Levin, Z., Pinsky, M., Phillips, V., Prabhakaran, T., Teller, A., van den Heever, S. C., and Yano, J.-I.: Representation of microphysical processes in cloud-resolving models: spectral (bin) microphysics versus bulk parameterization Rev. Geophys. 53, 247–322, http://dx.doi.org/ 10.1002/2014RG000468, 2015.

Koren, I., Feingold, G., and Remer, L. A.: The invigoration of deep convective clouds over the Atlantic: Aerosol effect, meteorology or retrieval artifact?, Atmos. Chem. Phys., 10, 8855–8872, doi:10.5194/acp-10-8855-2010a, 2010.

Korolev, A.: Reconstruction of the sizes of spherical particles from their shadow images. Part I: Theoretical considerations, J. Atmos. Oceanic Technol., 24, 376-389, doi:10.1175/JTECH1980.1, 2007.

Korolev, A., Khain, A., Pinsky, M., and French, J.: Theoretical study of mixing in liquid clouds – Part 1: Classical concepts, Atmos. Chem. Phys., 16, 9235-9254, doi:10.5194/acp-16-9235-2016, 2016.

Kuhn, U., Ganzeveld, L., Thielmann, A., Dindorf, T., Welling, M., Sciare, J., Roberts, G., Meixner, F. X., Kesselmeier, J., Lelieveld, J., Ciccioli, P., Lloyd, J., Trentmann, J., Artaxo, P., and Andreae, M. O.: Impact of Manaus City on the Amazon Green Ocean atmosphere: Ozone production, precursor sensitivity and aerosol load: Atmos. Chem. Phys., 10, 9251–9282, 2010.

Lamb, D., Hallett, J., and Sax, R.I.: Mechanistic limitations to the release of latent heat during the natural and artificial glaciation of deep convective clouds. Q.J.R. Meteorol. Soc., 107: 935-954, 1981.

Lance, S., Brock, C. A., Rogers, D., Gordon, J. A.: Water droplet calibration of the Cloud Droplet Probe (CDP) and inflight performance in liquid, ice and mixed-phase clouds during ARCPAC, Atmos. Meas. Tech., 3, 1683-1706, doi:10.5194/amt-3-1683-2010, 2010.

Lawson, R. P., Woods, S., and Morrison, H.: The microphysics of ice and precipitation development in tropical cumulus clouds. J. Atmos. Sci., 72, 2429–2445, doi:10.1175/JAS-D-14-0274.1, 2015.

Lee, S. S., Donner, L. J., Phillips, V. T. J., and Ming, Y.: Examination of aerosol effects on precipitation in deep convective clouds during the 1997 ARM summer experiment, Q. J. R. Meteorol. Soc., 134(634), 1201–1220, doi:10.1002/qj.287, 2008.

Li, Z., Niu, F., Fan, J., Liu, Y., Rosenfeld, D., and Ding, Y.: Long-term impacts of aerosols on the vertical development of clouds and precipitation. Nat. Geosci., 4, 888–894, doi:10.1038/ngeo1313, 2012.

Liu, C.: Rainfall contributions from precipitation systems with different sizes, convective intensities, and durations over the tropics and subtropics. J. Hydrometeor., 12, 394–412, 2011.

Lohmann, U., and Hoose, C.: Sensitivity studies of different aerosol indirect effects in mixed-phase clouds, Atmos. Chem. Phys., 9, 8917-8934, doi:10.5194/acp-9-8917-2009, 2009.

Luebke, A. E., Afchine, A., Costa, A., Grooß, J.-U., Meyer, J., Rolf, C., Spelten, N., Avallone, L. M., Baumgardner, D., and Krämer, M.: The origin of midlatitude ice clouds and the resulting influence on their microphysical properties, Atmos. Chem. Phys., 16, 5793-5809, doi:10.5194/acp-16-5793-2016, 2016.

Machado, L.A.T., Silva Dias, M. A. F., Morales, C., Fisch, G., Vila, D., Albrecht, R. I., Goodman, S. J., Calheiros, A. J. P., Biscaro, T., Kummerow, C., Cohen, J., Fitzjarrald, D., Nascimento, E. L., Sakamoto, M. S., Cunningham, C., Chaboureau, J.-P., Petersen, W. A., Adams, D. K., Baldini, L., Angelis, C. F., Sapucci, L. F., Salio, P., Barbosa, H. M. J., Landulfo, E., Souza, R. A. F., Blakeslee, R. J., Bailey, J., Freitas, S., Lima, W. F. A., and Tokay, A.: The Chuva Project: How Does Convection Vary across Brazil? Bull. Amer. Meteor. Soc., 95, 1365–1380, 2014.

Mallaun, C., Giez, A., and Baumann, R.: Calibration of 3-D wind measurements on a single-engine research aircraft, Atmos. Meas. Tech., 8(8), 3177–3196, doi:10.5194/amt-8-3177-2015, 2015.

Martin, S. T., Andreae, M. O., Artaxo, P., Baumgardner, D., Chen, Q., Goldstein, A. H., Guenther, A., Heald, C. L., Mayol-Bracero, O. L., McMurry, P. H., Pauliquevis, T., Pöschl, U., Prather, K. A., Roberts, G. C., Saleska, S. R., Silva Dias, M. A., Spracklen, D. V., Swietlicki, E., and Trebs, I.: Sources and properties of Amazonian aerosol particles, Rev. Geophys., 48, RG2002, 2010.

Martin, S. T., Artaxo, P., Machado, L. A. T., Manzi, A. O., Souza, R. A. F., Schumacher, C., Wang, J., Andreae, M. O., Barbosa, H. M. J., Fan, J., Fisch, G., Goldstein, A. H., Guenther, A., Jimenez, J. L., Pöschl, U., Silva Dias, M. A., Smith, J. N., and Wendisch, M.: Introduction: Observations and modeling

of the Green Ocean Amazon (GoAmazon2014/5), Atmos. Chem. Phys., 16, 4785-4797, doi:10.5194/acp-16-4785-2016, 2016.

McFarquhar, G. M., Hsieh, T., Freer, M., Mascio, J., and Jewett, B. F.: The characterization of ice hydrometeor gamma size distributions as volumes in N_0–λ–μ phase space: Implications for microphysical process modeling, J. Atmos. Sci., 72, 892–909, doi:10.1175/JAS-D-14-0011.1, 2015.

Milbrandt, J. A., and Yau, M. K.: A multimoment bulk microphysics parameterization. Part I: Analysis of the role of the spectral shape parameter, J. Atmos. Sci., 62, 3051–3064, 2005.

Molleker, S., Borrmann, S., Schlager, H., Luo, B., Frey, W., Klingebiel, M., Weigel, R., Ebert, M., Mitev, V., Matthey, R., Woiwode, W., Oelhaf, H., Dörnbrack, A., Stratmann, G., Grooß, J.-U., Günther, G., Vogel, B., Müller, R., Krämer, M., Meyer, J., and Cairo, F.: Microphysical properties of synoptic scale polar stratospheric clouds: in situ measurements of unexpectedly large HNO3 containing particles in the Arctic vortex, Atmos. Chem. Phys., 14, Atmos. Chem. Phys., 14, 10785-10801, doi:10.5194/acp-14-10785-2014, 2014.

Mossop, S.C.: The influence of drop size distribution on the production of secondary ice particles during graupel growth. Q. J. R. Meteorol. Soc. 104, 323–330, 1978.

Pinsky, M., Khain, A., Mazin, I., and Korolev, A.: Analytical estimation of droplet concentration at cloud base, J. Geophys. Res., 117, D18211, doi:10.1029/2012JD017753, 2012.

Pinsky, M., Khain, A., Korolev, A., and Magaritz-Ronen, L.: Theoretical investigation of mixing in warm clouds – Part 2: Homogeneous mixing, Atmos. Chem. Phys., 16, 9255-9272, doi:10.5194/acp-16-9255-2016, 2016a.

Pinsky, M., Khain, A., and Korolev, A.: Theoretical analysis of mixing in liquid clouds – Part 3: Inhomogeneous mixing, Atmos. Chem. Phys., 16, 9273-9297, doi:10.5194/acp-16-9273-2016, 2016b.

Riehl, H., and Malkus, J. S.: On the heat balance in the equatorial trough zone. Geophysica, 6, 503–538, 1958.

Pöhlker, C., Wiedemann, K., Sinha, B., Shiraiwa, M., Gunthe, S., Smith, M., Su, H., Artaxo, P., Chen, Q., Cheng, Y., Elbert, W., Gilles, M. K., Kilcoyne, A. L. D., Moffet, R. C., Weigand, M., Martin, S. T., Pöschl, U., and Andreae, M. O., Biogenic potassium salt particles as seeds for secondary organic aerosol in the Amazon: Science, 337, 1075-1078, 2012.

Pöhlker, M. L., Pöhlker, C., Ditas, F., Klimach, T., Hrabe de Angelis, I., Araújo, A., Brito, J., Carbone, S., Cheng, Y., Chi, X., Ditz, R., Gunthe, S. S., Kesselmeier, J., Könemann, T., Lavrič, J. V., Martin, S. T., Mikhailov, E., Moran-Zuloaga, D., Rose, D., Saturno, J., Su, H., Thalman, R., Walter, D., Wang, J., Wolff, S., Barbosa, H. M. J., Artaxo, P., Andreae, M. O., and Pöschl, U., Long-term observations of cloud condensation nuclei in the Amazon rain forest – Part 1: Aerosol size distribution, hygroscopicity, and new model parametrizations for CCN prediction: Atmos. Chem. Phys., 16, 15,709-15,740, doi:10.5194/acp-16-15709-2016, 2016.

Pöschl, U., Martin, S. T., Sinha, B., Chen, Q., Gunthe, S. S., Huffman, J. A., Borrmann, S., Farmer, D. K., Garland, R. M., Helas, G., Jimenez, J. L., King, S. M., Manzi, A., Mikhailov, E., Pauliquevis, T., Petters, M. D., Prenni, A. J., Roldin, P., Rose, D., Schneider, J., Su, H., Zorn, S. R., Artaxo, P., and Andreae, M. O.: Rainforest aerosols as biogenic nuclei of clouds and precipitation in the Amazon. Science, 329(5998), p. 1513-1516, 2010.

Prenni, A. J., Petters, M. D., Kreidenweis, S. M., Heald, C. L., Martin, S. T., Artaxo, P., Garland, R. M., Wollny, A. G., and Pöschl, U.: Relative roles of biogenic emissions and Saharan dust as ice nuclei in the Amazon Basin, Nat. Geosci., 2, 402–405, doi:10.1038/ngeo517, 2009.

Roberts, G. C., Nenes, A., Seinfeld, J. H., and Andreae, M. O.: Impact of biomass burning on cloud properties in the Amazon Basin. *J. Geophys. Res.*, **108**, 4062, doi:10.1029/2001JD000985, 2003.

Riehl, H., and Simpson, J. S.: On the heat balance in the equatorial trough zone, revisited. Contrib. Atmos. Phys., 52, 287–305, 1979.

Roberts, G.C., and Nenes, A.: A Continuous-Flow streamwise thermal-gradient CCN chamber for atmospheric measurements, Aerosol Sci. Technol., 39(3), 206–221, doi:10.1080/027868290913988, 2005.

Rosenfeld, D., and Woodley, W. L.: Deep convective clouds with sustained supercooled liquid water down to-37.5 o495 C,

Nature, 405, 440-442, 10.1038/35013030, 2000.

Rosenfeld, D., Lohmann, U., Raga, G. B., O'Dowd, C. D., Kulmala, M., Fuzzi, S., Reissell, A., and Andreae, M. O.: Flood or drought: How do aerosols affect precipitation?, Science, 321, 1309–1313, 2008.

Rosenfeld, D., Andreae, M. O., Asmi, A., Chin, M., de Leeuw, G., Donovan, D. P., Kahn, R., Kinne, S., Kivekäs, N., Kulmala, M., Lau, W., Schmidt, K. S., Suni, T., Wagner, T., Wild, M., and Quaas, J.: Global observations of aerosol-cloudprecipitation-climate interactions. Rev. Geophys., 52, 750–808, doi:10.1002/2013RG000441, 2014.

Saunders, C. P. R., Hosseini, A. S.: A laboratory study of the effect of velocity on Hallett–Mossop ice crystal multiplication. Atmos. Res. 59–60, 3–14, 2001.

Seifert, A., and Beheng, K. D.: A two-moment cloud microphysics parameterization for mixed-phase clouds. Part 2: Maritime vs. continental deep convective storms, Meteorol. Atmos. Phys., 92, 67–82, 2006.

Sun, J., Parisa, A., Ariya, H., Leighton, G., and Yau, M.K.: Modeling study of ice formation in warm-based precipitating shallow cumulus clouds. JAS 69, 3315–3335, 2012.

Tao, W.-K., Chen, J.-P., Li, Z., Wang, C., and Zhang, C.: Impact of aerosols on convective clouds and precipitation, Rev. Geophys., 50, RG2001, doi:10.1029/2011RG000369, 2012.

Talbot, R. W., Andreae, M. O., Andreae, T. W., and Harriss, R. C., Regional aerosol chemistry of the Amazon Basin during the dry season: J. Geophys. Res., 93, 1499-1508, 1988.

Talbot, R. W., Andreae, M. O., Berresheim, H., Artaxo, P., Garstang, M., Harriss, R. C., Beecher, K. M., and Li, S. M., Aerosol chemistry during the wet season in Central Amazonia: The influence of long-range transport: J. Geophys. Res., 95, 16,955-16,969, 1990.

Tas, E., Teller, A., Altaratz, O., Axisa, D., Bruintjes, R., Levin, Z., and Koren, I.: The relative dispersion of cloud droplets: its robustness with respect to key cloud properties, Atmos. Chem. Phys., 15, 2009-2017, doi:10.5194/acp-15-2009-2015, 2015.

Thompson, G., Rasmussen, R. M., and Manning, K.: Explicit forecasts of winter precipitation using an improved bulk microphysics scheme. Part I: Description and sensitivity analysis, Mon. Weather Rev., 132, 519–542, 2004.

Twomey, S.: Pollution and the planetary albedo. Atmos. Environ., 8, 1251–1256, doi:10.1016/0004-6981(74)90004-3, 1974.

Ulbrich, C. W.: Natural variations in the analytical form of the raindrop size distribution. *J. Climate Appl. Meteor.*, **22,** 1764–1775, 1983.

van den Heever, S. C., Carrió, G. G., Cotton, W. R., DeMott, P. J., and Prenni, A. J.: Impacts of nucleating aerosol on Florida storms. Part I: Mesoscale simulations. J. Atmos. Sci., 63, 1752–1775, doi:10.1175/JAS3713.1, 2006.

van den Heever, S. C., and Cotton, W. R.: Urban aerosol impacts on downwind convective storms, J. Appl. Meteorol. Climatol., 46, 828–850, 2007.

Vera, C., Higgins, W., Amador, J., Ambrizzi, T., Garreaud, R., Gochis, D., Gutzler, D., Lettenmaier, D., Marengo, J., Mechoso, C.R., Nogues-Paegle, J., Silva Diaz, P.L., and Zhang, C.: Towards a unified view of the American Monsoon System. J. Climate 19, 4977–5000, 2006.

Weigel, R., Spichtinger, P., Mahnke, C., Klingebiel, M., Afchine, A., Petzold, A., Krämer, M., Costa, A., Molleker, S., Reutter, P., Szakáll, M., Port, M., Grulich, L., Jurkat, T., Minikin, A., and Borrmann, S.: Thermodynamic correction of particle concentrations measured by underwing probes on fast-flying aircraft, Atmos. Meas. Tech., 9, 5135-5162, doi:10.5194/amt-9-5135-2016, 2016.

Wendisch, M., and J.-L. Brenguier (Eds.), 2013: Airborne Measurements for Environmental Research: Methods and Instruments. Wiley-VCH Verlag GmbH & Co. KGaA, Weinheim, Germany. ISBN: 978-3-527-40996-9. 655 pp., doi:10.1002/9783527653218.

Wendisch, M., Pöschl, U., Andreae, M. O., Machado, L. A. T., Albrecht, R., Schlager, H., Rosenfeld, D., Martin, S. T., Abdelmonem, A., Afchine, A., Araújo, A., Artaxo, P., Aufmhoff, H., Barbosa, H. M. J., Borrmann, S., Braga, R., Buchholz, B., Cecchini, M. A., Costa, A., Curtius, J., Dollner, M., Dorf, M., Dreiling, V., Ebert, V., Ehrlich, A., Ewald, F., Fisch, G., Fix, A., Frank, F., Fütterer, D., Heckl, C., Heidelberg, F., Hüneke, T., Jäkel, E., Järvinen, E., Jurkat, T., Kanter, S., Kästner, U., Kenntner, M., Kesselmeier, J., Klimach, T., Knecht, M., Kohl, R., Kölling, T., Krämer, M., Krüger, M., Krisna, T. C., Lavric, J. V., Longo, K., Mahnke, C., Manzi, A. O., Mayer, B., Mertes, S., Minikin, A., Molleker, S., Münch, S., Nillius, B., Pfeilsticker, K., Pöhlker, C., Roiger, A., Rose, D., Rosenow, D., Sauer, D., Schnaiter, M., Schneider, J., Schulz, C., de Souza, R. A. F., Spanu, A., Stock, P., Vila, D., Voigt, C., Walser, A., Walter, D., Weigel, R., Weinzierl, B., Werner, F., Yamasoe, M. A., Ziereis, H., Zinner, T., Zöger, M.: The ACRIDICON-CHUVA campaign: Studying tropical deep convective clouds and precipitation over Amazonia using the new German research aircraft HALO. Bull. Am. Meteorol. Soc., 97, 10, 1885-1908, http://dx.doi.org/10.1175/BAMS-D-14-00255.1, 2016.

Williams, E., Rosenfeld, D., Madden, N., Gerlach, J., Gears, N., Atkinson, L., Dunnemann, N., Frostrom, G., Antonio, M., Biazon, B., Camargo, R., Franca, H., Gomes, A., Lima, M., Machado, R., Manhaes, S., Nachtigall, L., Piva, H., Quintiliano, W., Machado, L., Artaxo, P., Roberts, G., Renno, N., Blakeslee, R., Bailey, J., Boccippio, D., Betts, A., Wolff, D., Roy, D., Halverson, J., Rickenbach, T., Fuentes, J., and Avelino, E., Contrasting convective regimes over the Amazon: Implications for cloud electrification: J. Geophys. Res., 107, 8082, doi:10.1029/2001JD000380, 2002.

Young, K.C.: The role of contact nucleation in ice phase initiation in clouds. J. Atmos. Sci., 31: 768-776, 1974.

Zhou, J., and Lau, K. M.: Does a Monsoon Climate Exist over South America? Journal of Climate, v. 11, p. 1020 – 1040, 1998.

Figure captions

Figure 1: Profile locations and trajectories of interest to this study. The ACRIDICON-CHUVA research flights were labeled chronologically from AC07 to AC20. The labels in the figure reflect the respective

flights where the cloud profiling section took place. The colors represent the different regions: green for remote Amazon, blue for near the Atlantic coast, and red for the Arc of Deforestation (different shades for clarity).

Figure 2: GOES-13 visible images for flights (a) ~~AC19~~M1, (b) ~~AC09~~RA1, (c) ~~AC18~~RA2, (d) ~~AC07~~AD1, (e) ~~AC12~~ AD2 and (f) ~~AC13~~AD3. Images are approximately 1 hour after the profile start time.

Figure 3: Conceptual drawing of the properties of the Gamma phase space in the warm layer of the clouds. The dotted gray line represents one trajectory through the phase space, representing the DSD evolution. P_1 is one DSD that grows by condensation and collision-coalescence to reach P_2. The displacement represented by the pseudo-force $\vec{F}$ is decomposed into two components - $\overrightarrow{F_{cd}}$ (condensational pseudo-force) and $\overrightarrow{F_{cl}}$ (collisional pseudo-force). Also shown are the two DSDs representative of points P_1 and P_2.

Figure 4: Average vertical profiles of potential temperature (a) and relative humidity (b) for flights over the Atlantic coast, remote Amazon, and Arc of Deforestation. The markers in the left vertical axis in (a) represent the altitude of the 0 °C isotherm for the different flights. Altitudes are relative to cloud base (*H*, negative values are below clouds). θ and RH are calculated as averages of level flight legs outside clouds.

Figure 5: Gamma phase space for flight ~~AC19~~ M1 over the coastal region. Small markers represent 1 Hz data, while bigger ones are averages for 200 m vertical intervals. The continuous black line represents a cubic spline fit for the averaged DSDs to illustrate its mean evolution. Altitudes are relative to cloud base (*H*).

Figure 6: Similar to Figure 5, but for flights ~~AC09~~ RA1 and ~~AC18~~ RA2 over the remote Amazon.

Figure 7: Similar to Figure 5, but for flights ~~AC07~~AD1, ~~AC12~~ AD2 and ~~AC13~~ AD3 over the Arc of Deforestation.

Figure 8: Observed trajectories for the clouds measured over the remote Amazon during flight ~~AC09~~ RA1 (continuous line) and over the Arc of Deforestation during flight ~~AC12~~ AD2 (dashed line). The numbers shown close to the observed trajectories start at 1 at cloud base and grow with altitude (the respective markers are colored according do altitude above cloud base, *H*). Their respective properties are presented in Tables 2 and 3.

Figure 9: Averaged DSDs and their respective Gamma fittings for some points in the trajectories of clouds measured over (a) the remote Amazon (flight ~~AC09~~RA1) and (b) the Arc of Deforestation (flight ~~AC12~~AD2).

Figure 10: Surfaces of constant N_d as calculated by the inversion of Eq. 6. The trajectories for the clouds measured during flights ~~AC09~~ RA1 (blue) and ~~AC12~~ AD2 (red) are also shown. Note that the axes are rotated for clarity.

Figure 11: Vertical profiles of the 1 Hz measurements of N_d, LWC, D_{eff} and ε for background clouds over the remote Amazon (a, c, e, g) and polluted clouds over the Arc of Deforestation (b, d, f, h). Updraft speeds are colored in log scale, corresponding to $0.1 \leq w \leq 5$ m s^{-1}. Horizontal black lines mark the 0 °C level. Magenta curves in (c) and (d) are the adiabatic water content profiles. H is relative to cloud base altitude.

Figure 12: Frequency of occurrence of NIXE-CAPS sphericity classifications for (a) the remote Amazon and (b) the Arc of Deforestation. "Sph (liquid)" stands for many only spherical (D < 50 µm) and predominantly spherical (D > 50 µm) hydrometeors, "Asph small (mixed phase)" for many predominantly spherical (D < 50 µm) and only aspherical (D > 50 µm) hydrometeors, and "Asph large (ice)" for only very few aspherical (D < 50 µm) and only aspherical (D > 50 µm) hydrometeors. Temperatures shown on the x-axis are the center for 6 °C intervals, which corresponds to roughly 1-km-thick layers.

Table captions

Table 1: General characteristics of the cloud profiling missions of interest to this study: condensation nuclei (N_{CN}) and CCN concentrations (N_{CCN}, with S = 0.48% ± 0.033%), cloud base and 0 °C isotherm altitude (H_{base} and $H_{0°C}$, respectively), start and end time and total number of DSDs collected. The data are limited to the lower 6 km of the clouds. The unit for N_{CN} and N_{CCN} is cm^{-3} and the unit for altitudes is in m. Profile start and end are given in local time. The names in the third column have the following meaning: M1 – Maritime 1; RA1 and RA2 – Remote Amazon 1 and Remote Amazon 2; AD1, AD2, and AD3 – Arc of Deforestation 1, Arc of Deforestation 2, and Arc of Deforestation 3.

Table 2: Properties of the points highlighted in Figure 8 for flight ~~AC09~~RA1. *H* is shown as the average of each of the 200-m vertical bins. The adiabatic fraction is defined as the ratio between the observed and adiabatic *LWC*. Adiabatic values for N_d, *LWC* and ε are shown below the respective observed quantities.

Table 3: Properties of the points highlighted in Figure 8 for flight ~~AC12~~AD2. *H* is shown as the average of each of the 200-m vertical bins. The adiabatic fraction is defined as the ratio between the observed and adiabatic *LWC*. Adiabatic values for N_d, *LWC* and ε are shown below the respective observed quantities.

Tables

Table 1: General characteristics of the cloud profiling missions of interest to this study: condensation nuclei (N_{CN}) and CCN concentrations (N_{CCN}, with S = 0.48% ± 0.033%), cloud base and 0 °C isotherm altitude (H_{base} and $H_{0°C}$, respectively), start and end time and total number of DSDs collected. The data are limited to the lower 6 km of the clouds. The unit for N_{CN} and N_{CCN} is cm^{-3} and the unit for altitudes is in m. Profile start and end are given in local time. The names in the third column have the following

meaning: M1 – Maritime 1; RA1 and RA2 – Remote Amazon 1 and Remote Amazon 2; AD1, AD2, and AD3 – Arc of Deforestation 1, Arc of Deforestation 2, and Arc of Deforestation 3.

Region	Flight	Name (this study)	N_{CN} (cm^{-3})	N_{CCN} (cm^{-3})	H_{base} (m)	$H_{0°C}$ (m)	Start	End	# DSDs
Atlantic Coast	AC19	M1	465	119	550	4651	13:17	14:57	630
Remote Amazon	AC09	RA1	821	372	1125	4823	11:30	14:21	665
	AC18	RA2	744	408	1650	4757	12:32	14:14	397
Arc of Deforestation	AC07	AD1	2498	1579	1850	4848	13:49	17:16	674
	AC12	AD2	3057	2017	2140	4938	12:55	15:16	381
	AC13	AD3	4093	2263	2135	4865	12:46	15:36	204

Formatado: Fonte: Não Itálico

Table 2: Properties of the points highlighted in Figure 8 for flight ~~AC09~~RA1. *H* is shown as the average of each of the 200-m vertical bins. The adiabatic fraction is defined as the ratio between the observed and adiabatic *LWC*. ~~Adiabatic values for N_d, *LWC* and ε are shown below the respective observed quantities.~~

Point	H	N_d	*LWC*	ε	D_{eff}	*T*	*UR*	*w*	*Adiabatic fraction*

	(m)	(cm^{-3})	($g\ m^{-3}$)		(μm)	(°C)	(%)	($m\ s^{-1}$)	
1c	100	214	0.079	0.19	9.2	19.9	81	0.84	0.31
2c	300	238	0.15	0.22	11.1	18.6	82	0.91	0.22
3c	500	218	0.25	0.24	13.8	17.5	83	1.43	0.30
4c	700	227	0.34	0.28	15.2	16.6	77	1.41	0.28
5c	1100	245	0.61	0.27	18.0	13.6	85	1.13	0.31
6c	1300	284	0.79	0.29	18.9	12.0	80	1.03	0.34
7c	1700	231	0.79	0.28	20.1	10.6	71	1.49	0.28
8c	2300	187	1.21	0.27	24.7	7.1	78	1.66	0.34
9c	3100	233	1.95	0.22	26.4	3.5	64	2.79	0.47
10c	3900	54	0.61	0.34	30.9	-1.2	39	1.08	0.13
11c	4100	49	0.31	0.36	25.6	-1.8	61	0.31	0.065
12c	4700	36	0.26	0.47	28.6	-4.8	67	1.30	0.053
13c	5300	39	0.42	0.40	31.4	-8.1	26	2.39	0.083
14c	5900	30	0.16	0.48	26.4	-11.4	33	3.27	0.032

Table 3: Properties of the points highlighted in Figure 8 for flight ~~AC12~~AD2. *H* is shown as the average of each of the 200-m vertical bins. The adiabatic fraction is defined as the ratio between the observed and adiabatic *LWC*. ~~Adiabatic values for N_d, *LWC* and ε are shown below the respective observed quantities.~~

Point	H (m)	N_d (cm^{-3})	LWC ($g\ m^{-3}$)	ε	D_{eff} (μm)	T (°C)	UR (%)	w ($m\ s^{-1}$)	*Adiabatic fraction*
1p	100	528	0.11	0.37	8.4	16.3	72	1.17	0.59
2p	300	960	0.27	0.31	8.8	15.5	64	1.02	0.72
3p	500	634	0.21	0.28	9.2	14.7	58	1.28	0.29
4p	700	597	0.29	0.27	10.4	12.4	59	0.57	0.24
5p	1300	543	0.34	0.29	11.5	6.9	65	1.13	0.15
6p	1900	1066	1.12	0.29	13.7	2.6	69	0.74	0.38
7p	2100	874	0.75	0.31	12.8	2.4	62	2.89	0.26
8p	2700	477	0.62	0.32	14.8	0.4	8	1.62	0.17
9p	2900	1271	1.95	0.32	15.7	0.2	5	9.36	0.52
10p	3300	1024	1.78	0.24	15.7	-1.5	3	5.68	0.44
11p	3700	137	0.25	0.24	16.0	-3.6	4	0.26	0.06

Figures

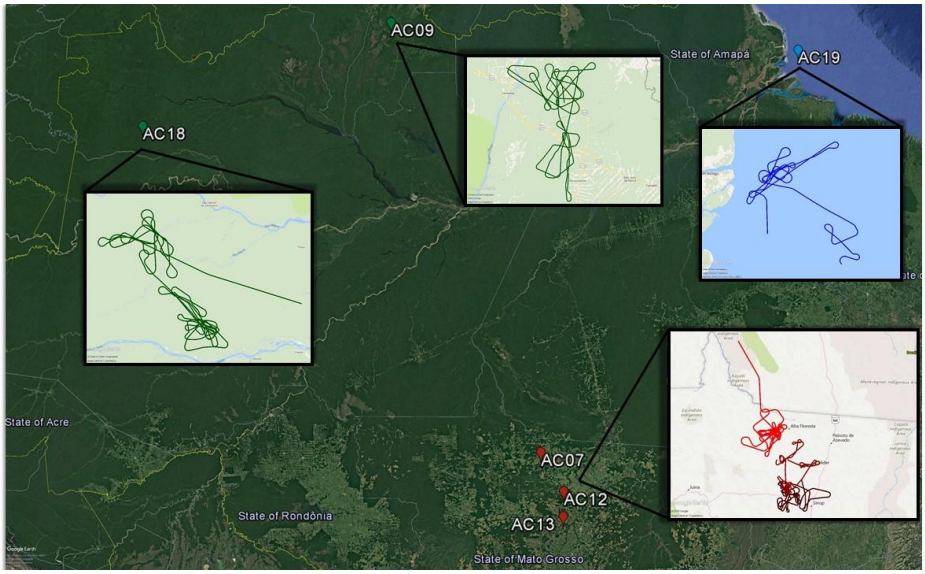

Figure 1: Profile locations and trajectories of interest to this study. The ACRIDICON-CHUVA research flights were labeled chronologically from AC07 to AC20. The labels in the figure reflect the respective flights where the cloud profiling section took place. The colors represent the different regions: green for remote Amazon, blue for near the Atlantic coast, and red for the Arc of Deforestation (different shades for clarity).

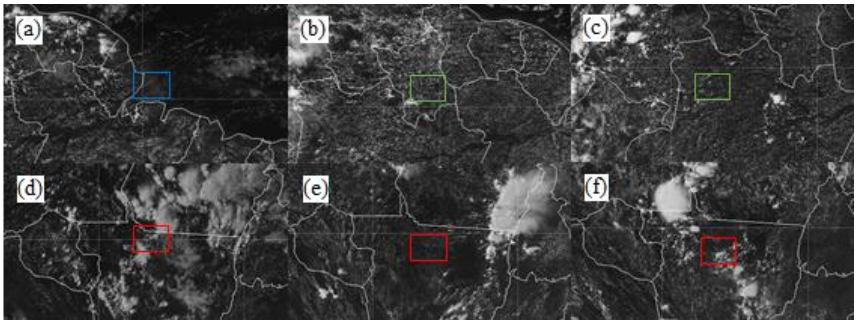

Figure 2: GOES-13 visible images for flights (a) ~~AC19~~M1, (b) ~~AC09~~RA1, (c) ~~AC18~~RA2, (d) ~~AC07~~AD1, (e) ~~AC12~~ AD2 and (f) ~~AC13~~AD3. Images are approximately 1 hour after the profile start time.

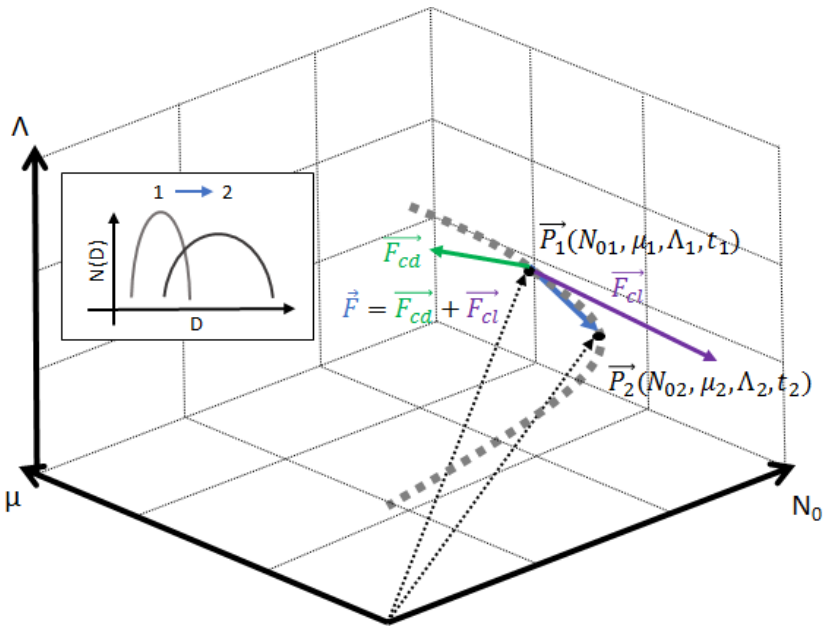

Figure 3: Conceptual drawing of the properties of the Gamma phase space in the warm layer of the clouds. The dotted gray line represents one trajectory through the phase space, representing the DSD evolution. P_1 is one DSD that grows by condensation and collision-coalescence to reach P_2. The displacement represented by the pseudo-force $\vec{F}$ is decomposed into two components - $\overrightarrow{F_{cd}}$ (condensational pseudo-force) and $\overrightarrow{F_{cl}}$ (collisional pseudo-force). Also shown are the two DSDs representative of points P_1 and P_2.

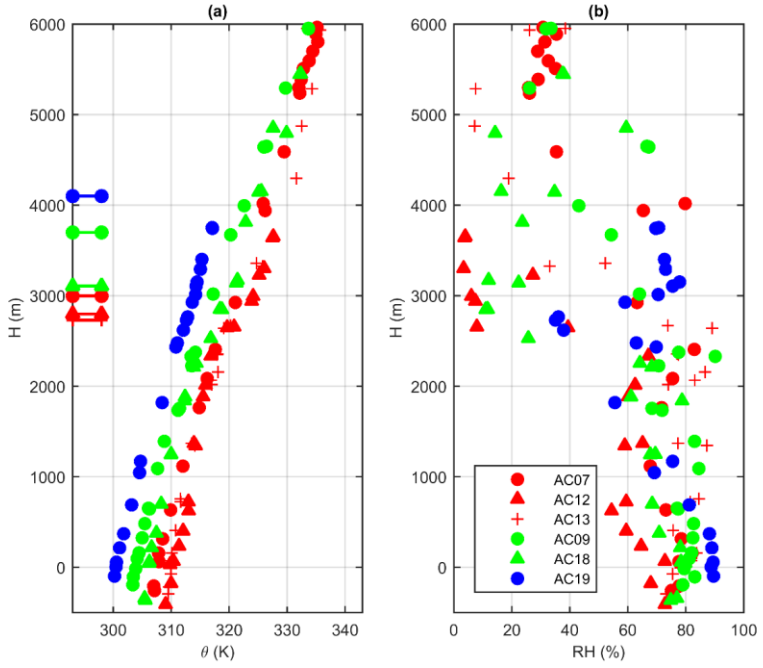
(a)
(b)
H (m)
θ (K)
RH (%)
AC07
AC12
AC13
AC09
AC18
AC19

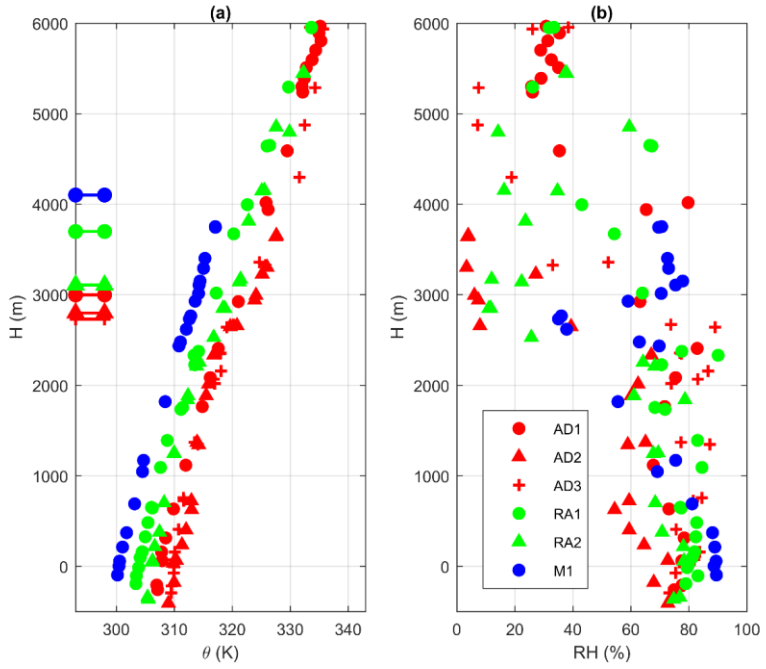

Figure 4: Average vertical profiles of potential temperature (a) and relative humidity (b) for flights over the Atlantic coast, remote Amazon, and Arc of Deforestation. The markers in the left vertical axis in (a) represent the altitude of the 0 °C isotherm for the different flights. Altitudes are relative to cloud base (*H*, negative values are below clouds). θ and RH are calculated as averages of level flight legs outside clouds.

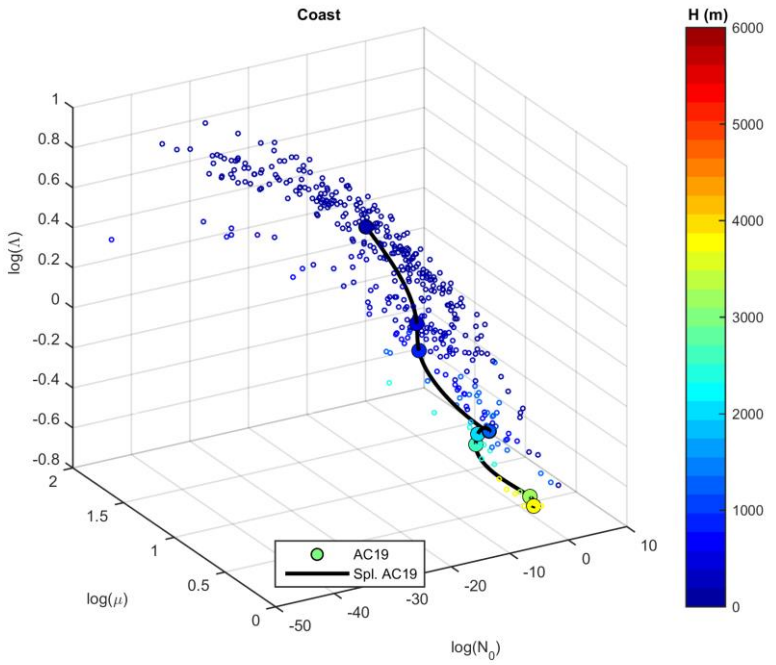
Coast
H (m)
6000
5000
4000
3000
2000
1000
0
log(Λ)
1
0.8
0.6
0.4
0.2
0
-0.2
-0.4
-0.6
-0.8
log(μ)
2
1.5
1
0.5
0
log(N0)
10
0
-10
-20
-30
-40
-50
AC19
Spl. AC19

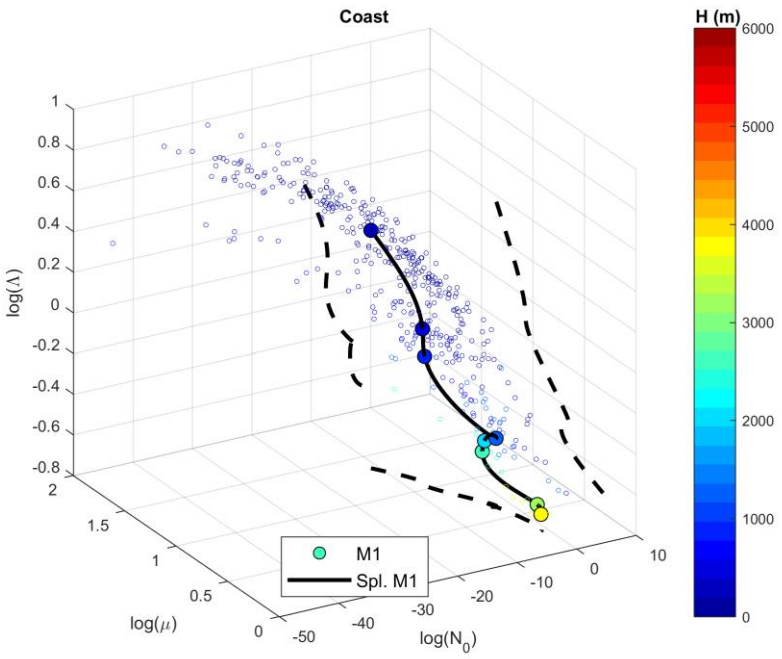

Figure 5: Gamma phase space for flight ~~AC19~~ M1 over the coastal region. Small markers represent 1 Hz data, while bigger ones are averages for 200 m vertical intervals. The continuous black line represents a cubic spline fit for the averaged DSDs to illustrate its mean evolution. Dashed lines represent its projections in the three planes. Altitudes are relative to cloud base (*H*).

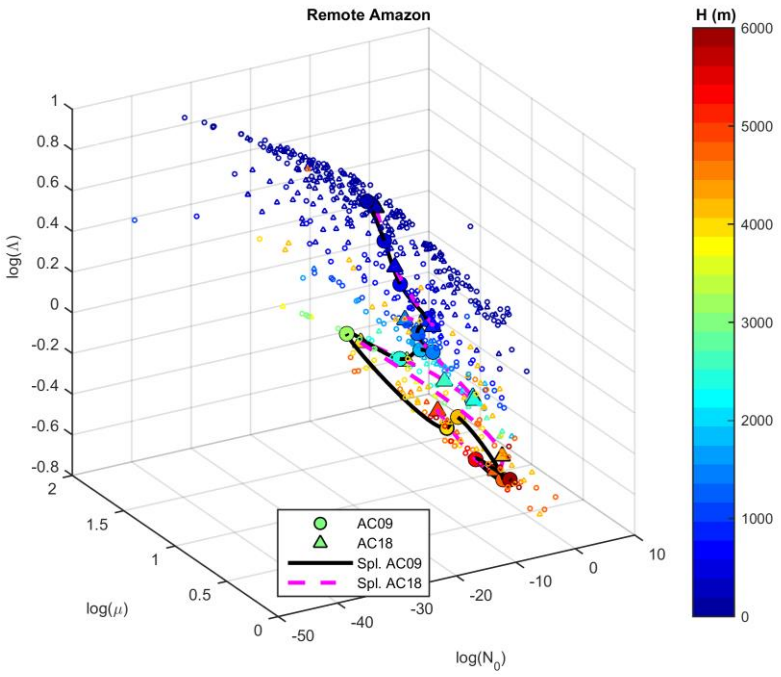
Remote Amazon
H (m)
6000
5000
4000
3000
2000
1000
0
log(Λ)
1
0.8
0.6
0.4
0.2
0
-0.2
-0.4
-0.6
-0.8
log(μ)
2
1.5
1
0.5
0
log(N0)
-50
-40
-30
-20
-10
0
10
AC09
AC18
Spl. AC09
Spl. AC18

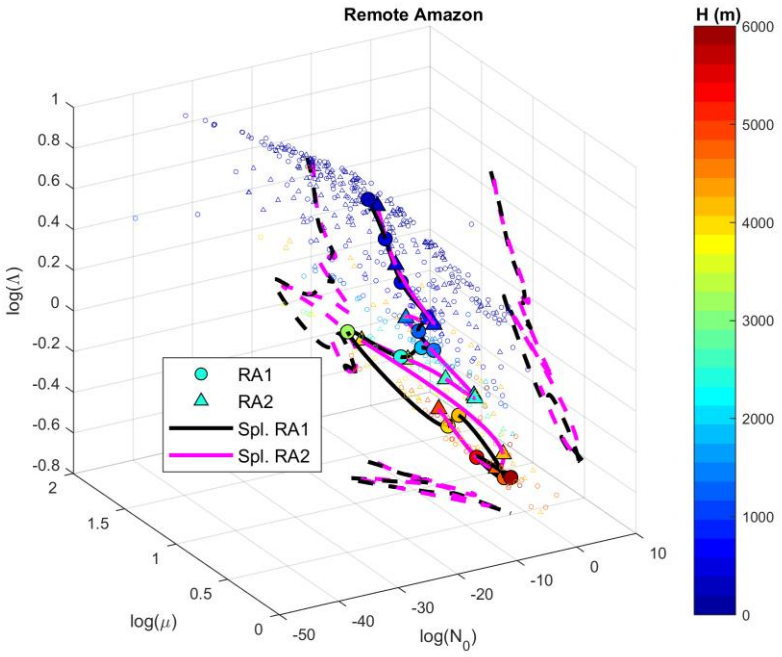

Figure 6: Similar to Figure 5, but for flights ~~AC09~~ RA1 and ~~AC18~~ RA2 over the remote Amazon.

Formatado: Português (Brasil)

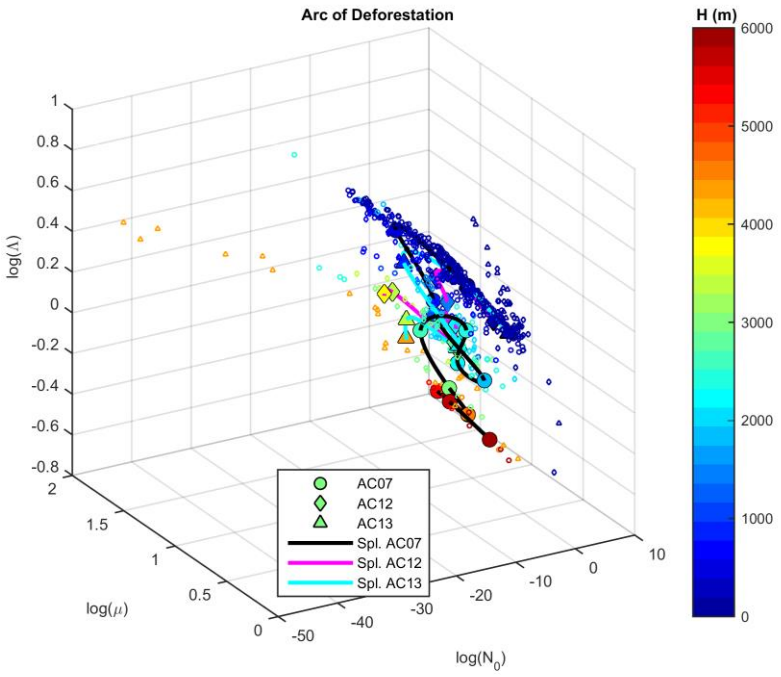
Arc of Deforestation
H (m)
6000
5000
4000
3000
2000
1000
0
log(Λ)
1
0.8
0.6
0.4
0.2
0
-0.2
-0.4
-0.6
-0.8
log(μ)
2
1.5
1
0.5
0
log(N0)
-50
-40
-30
-20
-10
0
10
AC07
AC12
AC13
Spl. AC07
Spl. AC12
Spl. AC13

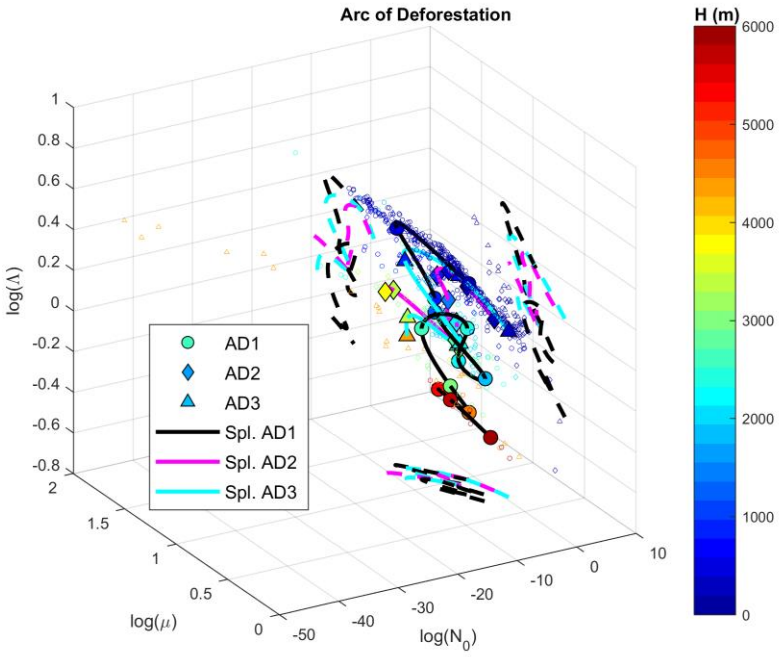

Figure 7: Similar to Figure 5, but for flights ~~AC07~~AD1, ~~AC12~~ AD2 and ~~AC13~~ AD3 over the Arc of Deforestation.

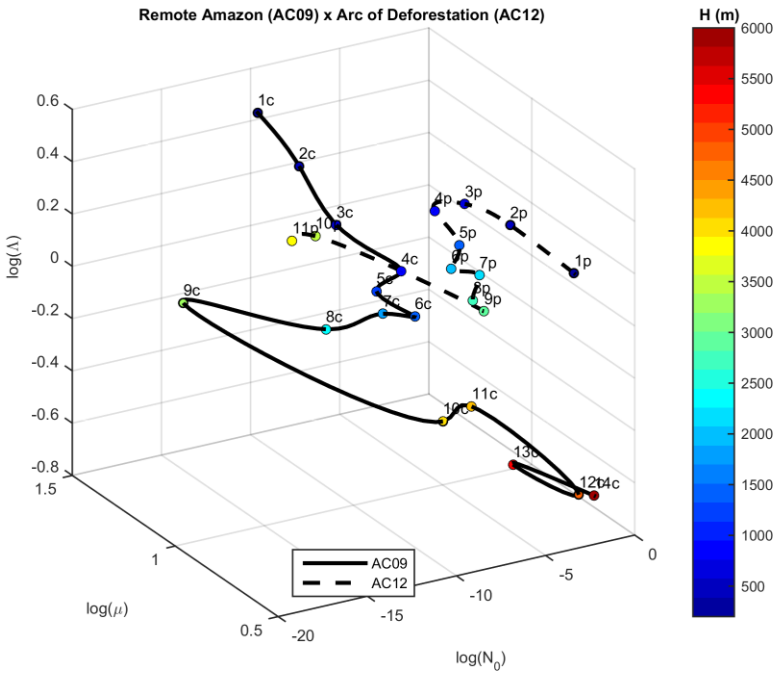
Remote Amazon (AC09) x Arc of Deforestation (AC12)
H (m)
6000
5500
5000
4500
4000
3500
3000
2500
2000
1500
1000
500
log(Λ)
0.6
0.4
0.2
0
-0.2
-0.4
-0.6
-0.8
log(μ)
1.5
1
0.5
log(N0)
0
-5
-10
-15
-20
AC09
AC12
1c
2c
3c
4c
5c
6c
7c
8c
9c
10c
11c
12c
13c
14c
1p
2p
3p
4p
5p
6p
7p
8p
9p
10p
11p

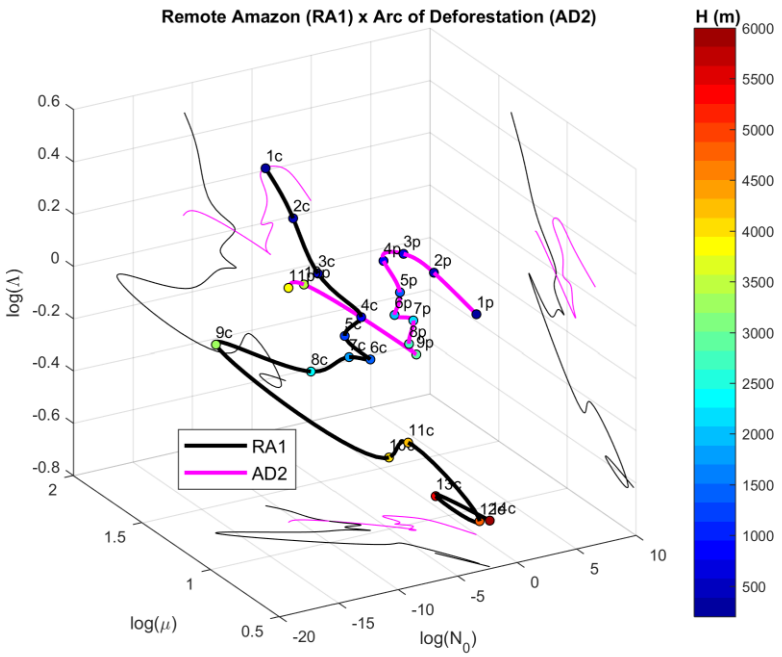

Figure 8: Observed trajectories for the clouds measured over the remote Amazon during flight ~~AC09~~ RA1 (continuous line) and over the Arc of Deforestation during flight ~~AC12~~ AD2 (dashed line). The numbers shown close to the observed trajectories start at 1 at cloud base and grow with altitude (the respective markers are colored according do altitude above cloud base, *H*). Their respective properties are presented in Tables 2 and 3.

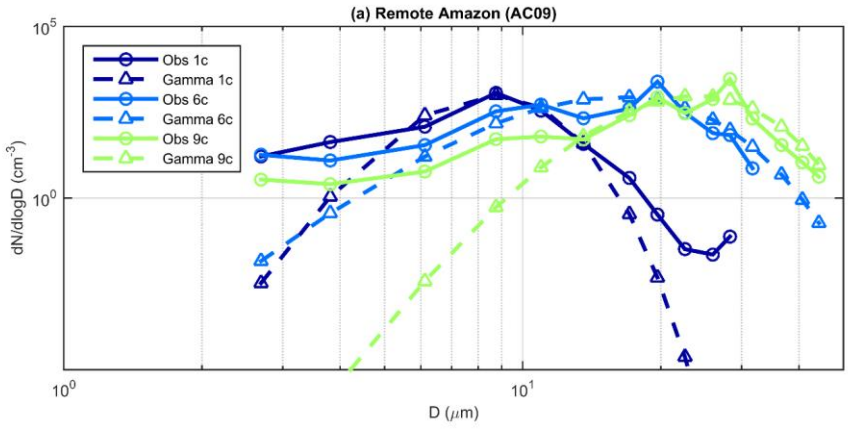
(a) Remote Amazon (AC09)
Obs 1c
Gamma 1c
Obs 6c
Gamma 6c
Obs 9c
Gamma 9c
dN/dlogD (cm^{-3})
D (μm)

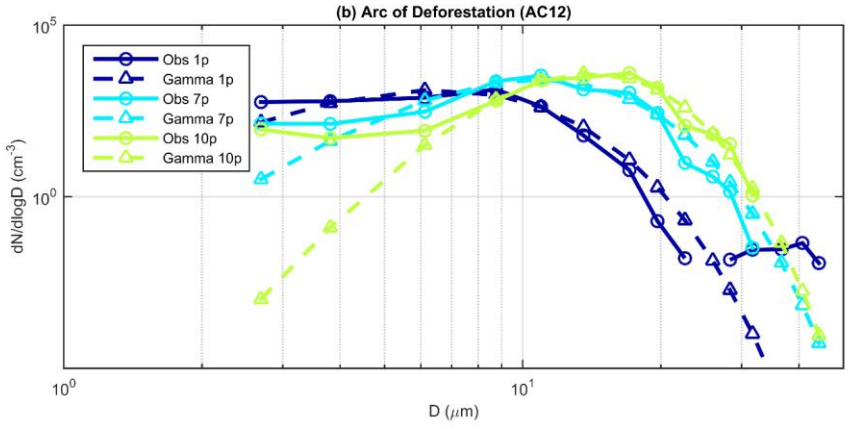
(b) Arc of Deforestation (AC12)
Obs 1p
Gamma 1p
Obs 7p
Gamma 7p
Obs 10p
Gamma 10p
dN/dlogD (cm^{-3})
D (μm)

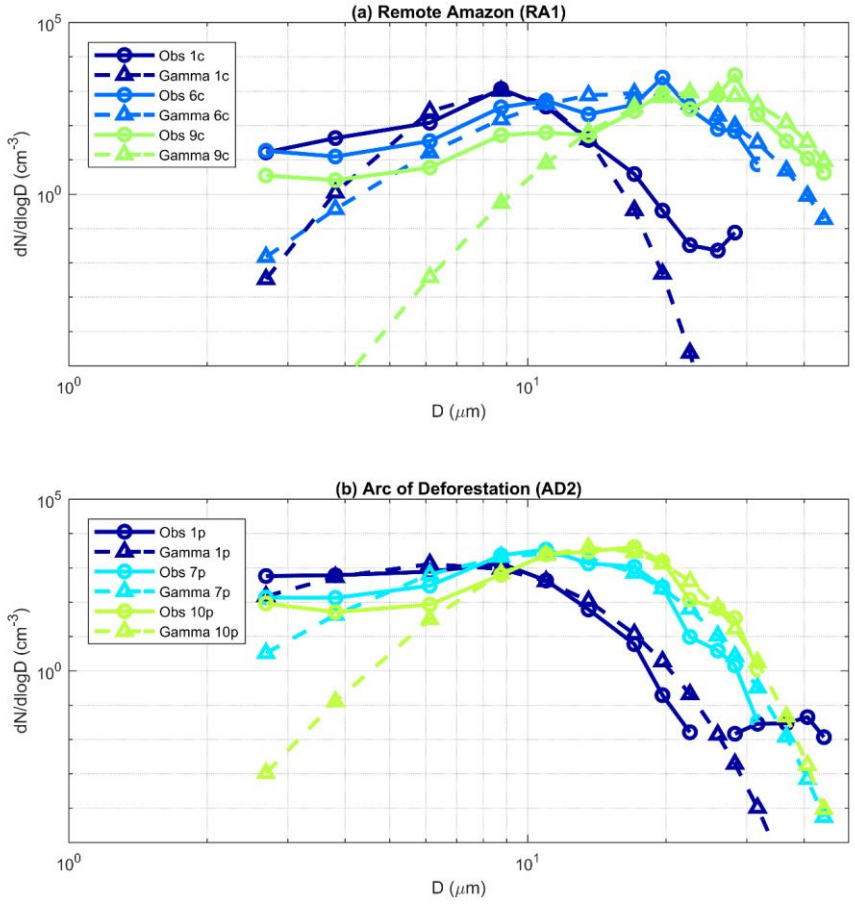

Figure 9: Averaged DSDs and their respective Gamma fittings for some points in the trajectories of clouds measured over (a) the remote Amazon (flight ~~AC09~~RA1) and (b) the Arc of Deforestation (flight ~~AC12~~AD2).

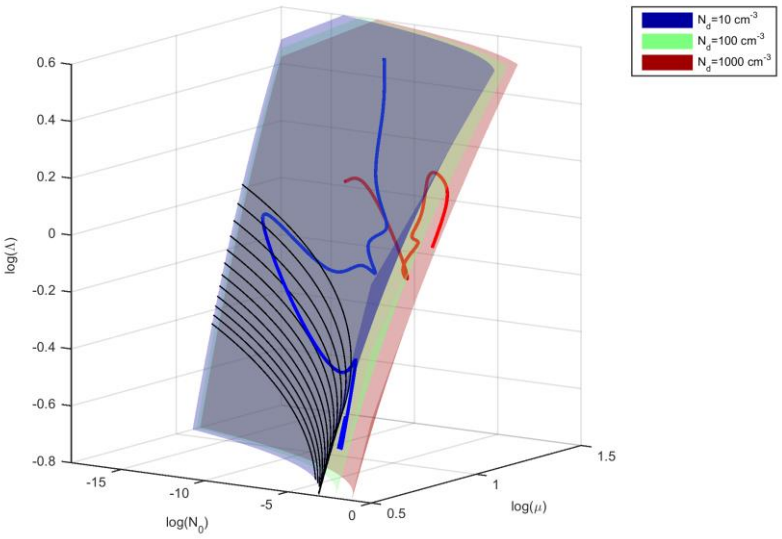

Figure 10: Surfaces of constant N_d as calculated by the inversion of Eq. 6. The trajectories for the clouds measured during flights ~~AC09~~ RA1 (blue) and ~~AC12~~ AD2 (red) are also shown. Note that the axes are rotated for clarity.

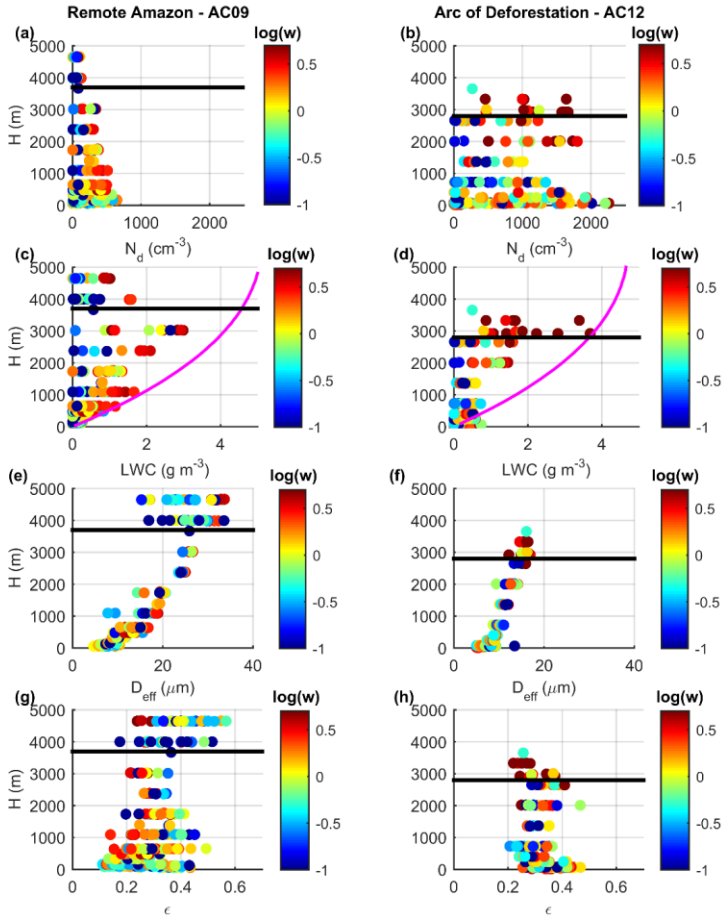
Remote Amazon - AC09
Arc of Deforestation - AC12
(a)
(b)
(c)
(d)
(e)
(f)
(g)
(h)
log(w)
H (m)
N_d (cm^-3)
LWC (g m^-3)
D_eff (μm)
ε

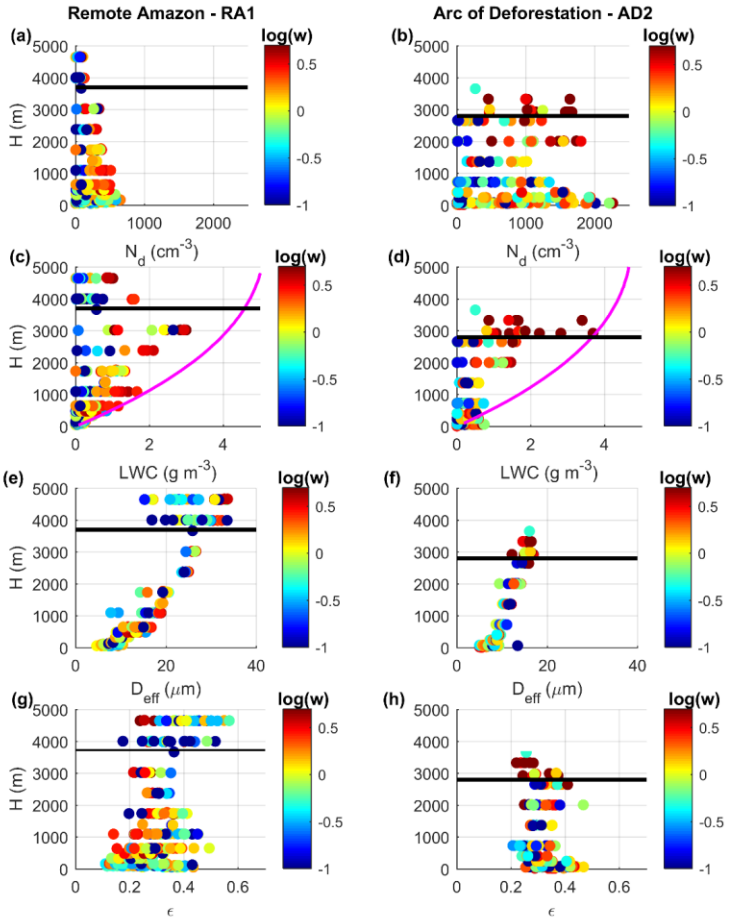

Figure 11: Vertical profiles of the 1 Hz measurements of N_d, LWC, D_{eff} and ε for background clouds over the remote Amazon (a, c, e, g) and polluted clouds over the Arc of Deforestation (b, d, f, h). Updraft speeds are colored in log scale, corresponding to $0.1 \leq w \leq 5$ m s^{-1}. Horizontal black lines mark the 0

°C level. Magenta curves in (c) and (d) are the adiabatic water content profiles. *H* is relative to cloud base altitude.

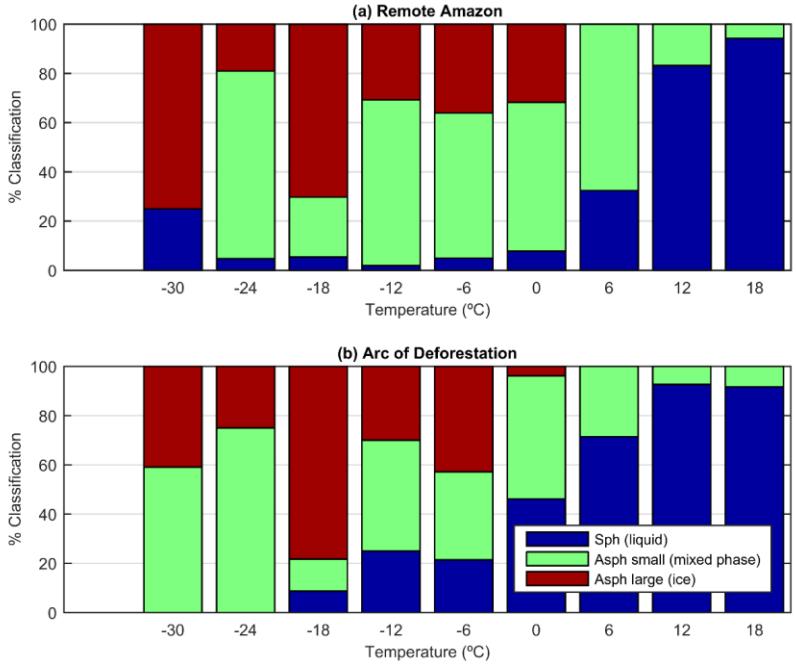

Figure 12: Frequency of occurrence of NIXE-CAPS sphericity classifications for (a) the remote Amazon and (b) the Arc of Deforestation. "Sph (liquid)" stands for many only spherical (D < 50 µm) and predominantly spherical (D > 50 µm) hydrometeors, "Asph small (mixed phase)" for many predominantly spherical (D < 50 µm) and only aspherical (D > 50 µm) hydrometeors, and "Asph large (ice)" for only very few aspherical (D < 50 µm) and only aspherical (D > 50 µm) hydrometeors. Temperatures shown on the x-axis are the center for 6 °C intervals, which corresponds to roughly 1-km-thick layers.